

UC Irvine

UC Irvine Previously Published Works

Title

Exposure to quasi-ultrafine particulate matter accelerates memory impairment and Alzheimer's disease-like neuropathology in the AppNL-G-F knock-in mouse model

Permalink

<https://escholarship.org/uc/item/6c1988s0>

Journal

Toxicological Sciences, 193(2)

ISSN

1096-6080

Authors

Kilian, Jason G
Mejias-Ortega, Marina
Hsu, Heng-Wei
et al.

Publication Date

2023-05-31

DOI

10.1093/toxsci/kfad036

Peer reviewed

Exposure to quasi-ultrafine particulate matter accelerates memory impairment and Alzheimer's disease-like neuropathology in the *App*^{NL-G-F} knock-in mouse model

Jason G. Kilian,^{1,2} Marina Mejias-Ortega,^{1,3,4} Heng-Wei Hsu,^{1,2} David A. Herman,¹ Janielle Vidal ,^{1,2} Rebecca J. Arechavala,¹ Samantha Renusch,¹ Hansal Dalal,¹ Irene Hasen,¹ Amanda Ting,¹ Carlos J. Rodriguez-Ortiz,^{1,2} Siok-Lam Lim,^{1,2} Xiaomeng Lin,¹ Joan Vu,^{1,2} Takashi Saito,⁵ Takaomi C. Saido,⁶ Michael T. Kleinman,¹ Masashi Kitazawa^{1,2*}

¹Department of Environmental and Occupational Health, Center for Occupational and Environmental Health (COEH), University of California, Irvine, California 92697-1830, USA

²Institute for Memory Impairments and Neurological Disorders (UCI MIND), University of California, Irvine, California 92697, USA

³Department of Cell Biology, Genetics and Physiology, Facultad de Ciencias, Instituto de Investigacion Biomedica de Malaga-IBIMA, Universidad de Malaga, Malaga, Spain,

⁴Centro de Investigación Biomedica en Red sobre Enfermedades Neurodegenerativas (CIBERNED), Madrid, Spain,

⁵Department of Neurocognitive Science, Institute of Brain Science, Nagoya City University, Nagoya, Japan

⁶Laboratory for Proteolytic Neuroscience, RIKEN Center for Brain Science, Wako, Japan

*To whom correspondence should be addressed at Department of Environmental and Occupational Health, Center for Occupational and Environmental Health (COEH), University of California, 856 Health Sciences Quad, suite 3200, Irvine, CA 92697-1830. E-mail: kitazawa@uci.edu.

Abstract

Exposure to traffic-related air pollution consisting of particulate matter (PM) is associated with cognitive decline leading to Alzheimer's disease (AD). In this study, we sought to examine the neurotoxic effects of exposure to ultrafine PM and how it exacerbates neuronal loss and AD-like neuropathology in wildtype (WT) mice and a knock-in mouse model of AD (*App*^{NL-G-F/+}-KI) when the exposure occurs at a prepathologic stage or at a later age with the presence of neuropathology. *App*^{NL-G-F/+}-KI and WT mice were exposed to concentrated ultrafine PM from local ambient air in Irvine, California, for 12 weeks, starting at 3 or 9 months of age. Particulate matter-exposed animals received concentrated ultrafine PM up to 8 times above the ambient levels, whereas control animals were exposed to purified air. Particulate matter exposure resulted in a marked impairment of memory tasks in prepathologic *App*^{NL-G-F/+}-KI mice without measurable changes in amyloid- β pathology, synaptic degeneration, and neuroinflammation. At aged, both WT and *App*^{NL-G-F/+}-KI mice exposed to PM showed a significant memory impairment along with neuronal loss. In *App*^{NL-G-F/+}-KI mice, we also detected an increased amyloid- β buildup and potentially harmful glial activation including ferritin-positive microglia and C3-positive astrocytes. Such glial activation could promote the cascade of degenerative consequences in the brain. Our results suggest that exposure to PM impairs cognitive function at both ages while exacerbation of AD-related pathology and neuronal loss may depend on the stage of pathology, aging, and/or state of glial activation. Further studies will be required to unveil the neurotoxic role of glial activation activated by PM exposure.

Keywords: Alzheimer's disease; air pollution; inflammation; neuronal loss; mouse model

Air pollution is a growing threat around the world and results from a variety of factors including urbanization, industrialization, slash-and-burn agriculture, climate change-driven wildfire, and desertification. The World Health Organization (WHO) estimates more than 90% of the worldwide population live in areas with poor air quality, and as many as 40% United States residents could be exposed continuously to unhealthy air based on current WHO standards (Peeples, 2020). In particular, under-represented minorities are disproportionately exposed to polluted air in the United States, posing significant health disparities (Bowe *et al.*, 2019; Tessum *et al.*, 2021). Although cardiopulmonary and cardiovascular morbidity is a well-documented health impact caused by exposure to polluted air and is considered the second largest noncommunicable disease (Peeples, 2020), in recent years,

multiple epidemiologic studies unveil a substantially greater risk for cognitive decline, dementia, and particularly Alzheimer's disease (AD) among elderly living in areas with heavy air pollution (Cacciottolo *et al.*, 2017; Carey *et al.*, 2018; Chang *et al.*, 2014; Chen and Schwartz, 2009; Gatto *et al.*, 2014; Kilian and Kitazawa, 2018; Oudin *et al.*, 2016; Power *et al.*, 2011; Ranft *et al.*, 2009; Shi *et al.*, 2020; Weuve *et al.*, 2012). The estimated risk of late-life exposure to air pollution for AD is predicted to be equivalent to or greater than that from traumatic brain injury, hypertension, or obesity in midlife (Livingston *et al.*, 2020), all of which are well studied risk factors for AD. However, key underlying mechanisms by which air pollution, or its specific toxic constituent, instigates neurodegeneration and causes the clinical onset of AD remain largely undetermined.

Ambient air pollution is highly heterogeneous and contains various toxic chemicals and elements. Among them, particulate matter (PM) is the major toxic constituent and is monitored as a primary indicator of air quality (Karagulian et al., 2015; Mazzei et al., 2008). Particulate matter toxicity has been extensively investigated in cardiovascular and pulmonary diseases based on its size: coarse (aerodynamic diameter $<10\ \mu\text{m}$), fine ($<2.5\ \mu\text{m}$) and ultrafine ($<0.1\ \mu\text{m}$), and chemicals associated with it, such as elemental metals, minerals, volatile organic compounds, and polycyclic aromatic hydrocarbons. The PM is generated directly from combustion of fossil fuels and wastes or indirectly by a series of photo-chemical reactions and nucleation in the atmosphere (Zhang et al., 2015). Fine and ultrafine PM and its neurotoxicity are of particular interest as they are the most abundant PM fraction compared with the total number of atmospheric PM; ultrafine PM can translocate from the lung directly to the bloodstream and able to cross the blood-brain barrier (BBB) via olfactory epithelium (Block and Calderon-Garciduenas, 2009; Gonzalez-Maciel et al., 2017; Oberdorster et al., 2004). Recent animal studies have found exposure to fine and ultrafine PM can accelerate AD-like neuropathology, neuronal loss, neuroinflammation, or cognitive decline (Bhatt et al., 2015; Cacciottolo et al., 2017; Campbell et al., 2005, 2009; Fonken et al., 2011; Haghani et al., 2020; Kim et al., 2012; Kleinman et al., 2008; Morgan et al., 2011). These studies suggest that PM exposure perturbs various pathologic mechanisms, such as inflammatory homeostasis (Fonken et al., 2011; Guerra et al., 2013; Haghani et al., 2020; Woodward et al., 2017) and APP metabolism (Bhatt et al., 2015; Cacciottolo et al., 2017). However, pivotal neurotoxic mechanisms by which PM exposure accelerates these hallmark pathologies are still ambiguous, and it remains unconfirmed if the neurotoxic effects of PM are consistent across the ages when exposed. Here, we report subchronic exposure to concentrated quasi-ultrafine PM significantly impaired cognition of mice at prepathologic and later ages. In addition, exacerbated neuronal loss, AD-like neuropathology and potentially harmful glial activation leading to neurodegeneration were observed in a mouse model of AD exposed to PM at an older age. Our findings suggest that neurotoxic activation of glial cells elicited by PM exposure in aged mice triggers the cascade of neurodegenerative mechanisms leading to accelerated development of AD phenotypes.

Materials and methods

Animals

All experiments were performed in accordance with the Institutional Animal Care and Use Committee at the University of California, Irvine. Mice were housed on a 12-h light-dark cycle with feed and water *ad libitum*. Humanized APP with the Swedish, Arctic, and Iberian mutations (*App*^{NL-G-F/+}-KI) mice in the C57BL/6J background were obtained from the RIKEN Institute (Japan) and maintained as heterozygous *App*^{NL-G-F/+}-KI by crossing with C57BL/6J mice (Saito et al., 2014). C57BL/6J male and female mice were obtained from Jackson Laboratory (Bar Harbor, Maine). For young, prepathologic animal exposure, 24 *App*^{NL-G-F/+}-KI mice (12 males and 12 females, divided evenly into the 2 groups—purified air group or concentrated PM group) were at 3 months of age when the exposure started in August 2017. For aged animal exposure, 40 *App*^{NL-G-F/+}-KI and 40 wildtype C57BL/6J (WT) mice were at 9 months of age when the exposure started in February 2019. Mice were divided evenly at 10 male and 10 female mice per group for 2 groups (purified air or concentrated PM).

Exposure paradigm

Ambient particles in the area around the UC Irvine area in Orange County, California with particle diameters smaller than $10\ \mu\text{m}$ (mixture of coarse, fine, and ultrafine particles, herein referred as PM) were concentrated using a versatile aerosol concentration and enrichment system (VACES) coupled with a high flow rate slit impactor as previously described (Herman et al., 2020; Kim, 2001; Misra et al., 2002). The VACES consists of size selective inlets, saturator/chiller modules that supersaturate the aerosol with water vapor causing ultrafine particles to grow to a size that can be inertially separated using a virtual impactor, and diffusion drier modules that remove excess water vapor and returns the aerosol to a size distribution and relative humidity similar to that observed in the ambient environment. The system can enrich the concentration of particles in the $0.02\text{--}10\ \mu\text{m}$ size range by a factor of up to $10\times$ ambient, depending on output flow rate (Herman et al., 2020; Luderer et al., 2022). Purified air during the exposures was generated using potassium permanganate-impregnated alumina beads, activated carbon, and high-efficiency particulate air filters. The VACES system is located adjacent to a major roadway in Irvine, CA, and exposure occurs over morning commute hours to emphasize motor vehicle associated PM. Starting at 3 or 9 months of age, *App*^{NL-G-F/+}-KI mice or WT mice were exposed to either purified air or concentrated PM. Animals were exposed in whole-body exposure chambers for 5 h per day (from 7:30 AM to 12:30 PM local time, which captured the period of maximum PM concentration during the day), 4 days per week (Tuesday-Friday) for 12 weeks (Figure 1A). The atmospheric pressure, temperatures ($23.9 \pm 2.8^\circ\text{C}$), and flow rates (2 liter per minute) within whole-body chambers were monitored every 15 min during each exposure period; animals were also monitored for signs of distress. Animals were then sacrificed following completion of the cognitive assessment.

PM measurement

Real-time particle measurements were obtained from the purified air, PM, and ambient atmospheres during exposures. Particle number concentration was collected using a condensation particle counter (Model 3022, TSI, Shoreview, Minnesota). Integrated particle mass concentrations were obtained using an optical mass monitor (DustTrak DRX, TSI). All data were averaged weekly \pm standard error of the mean.

Cognitive assessments

Animals were evaluated in object location memory (OLM) and object recognition memory (ORM) tasks. The OLM was performed during week 9 of the PM exposure. The ORM was run following a 1-week break period after OLM testing. Both ORM and OLM assessments were performed based on a previously described protocol (Vogel-Ciernia and Wood, 2014). For both tests, animals were habituated to the test arena for 6 days, 5 min per day, and then exposed to 2 identical objects for 10 min for training. Different base objects were used for ORM and OLM acquisition. Testing occurred 24 h following training. In the OLM task, one of the 2 objects was moved to a new location, whereas for ORM, one object was replaced with a novel object. Replaced or moved objects alternated between mice. Mice could explore during the test for 5 min. Both test and training exploration were recorded, and at least 2 examiners scored animal performance in a blinded manner. The total time spent exploring each object—determined as time with the animal's nose was within 1 cm and pointing directly towards the object—was counted as exploration. Time exploring each of the 2 objects was summed to obtain total

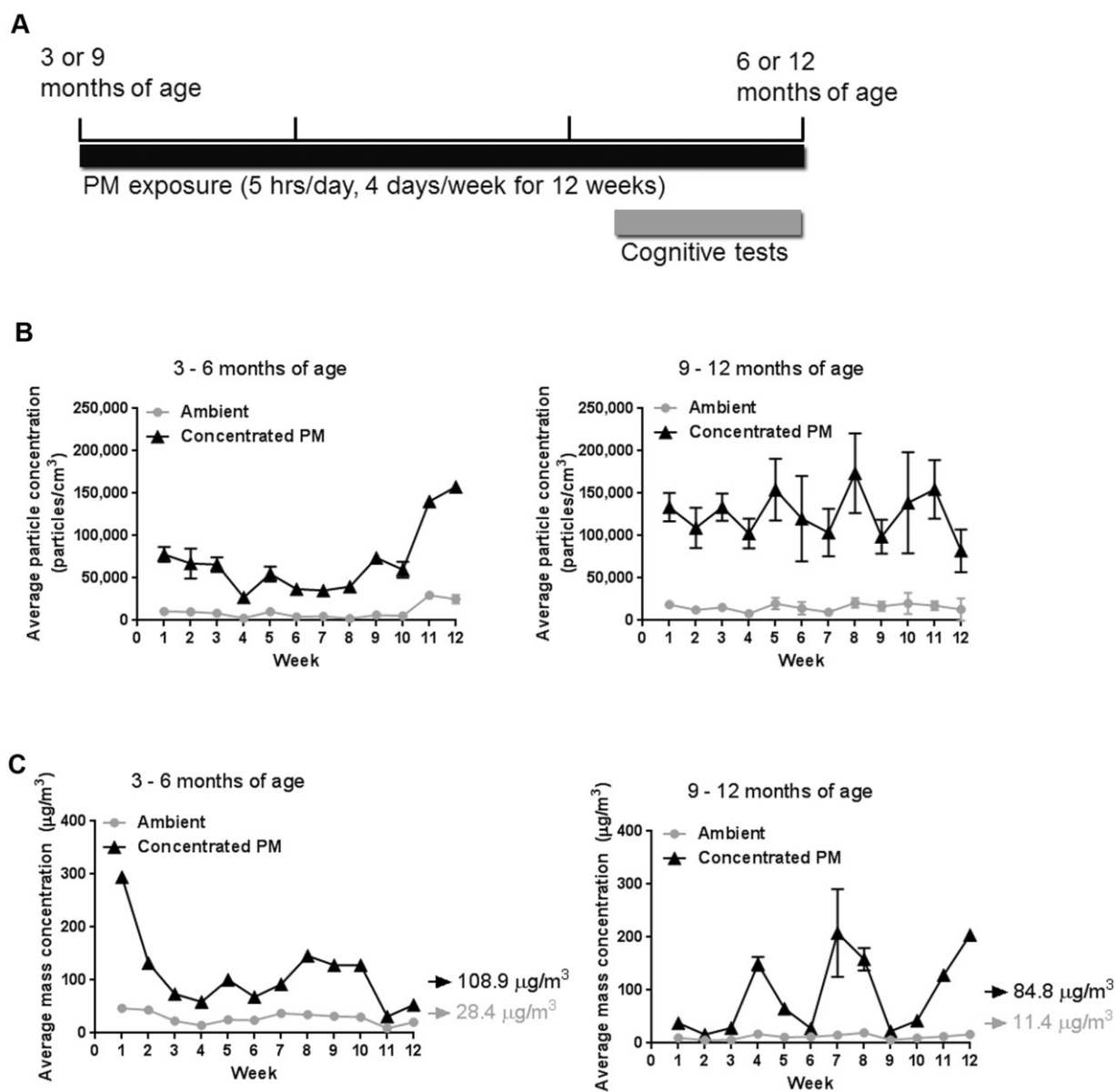


Figure 1. Particulate matter exposure scheme and average PM concentration during the 12-week exposure. A, Schematic diagram of PM exposure on animals. In the last 3 weeks, a battery of cognitive tests was performed in the afternoon while animals continued to be exposed in the morning. B, The average particle concentration of 3–6 months exposure (left) or 9–12 months exposure (right) in particle/m³. C, The average particle mass concentration of 3–6 months exposure (left) or 9–12 months exposure (right) in µg/m³.

exploration time. Animals showing a strong preference for exploring one object over the other during the acquisition phase were removed from the final analysis pool. Each discrimination index was calculated as the difference between the average time spent exploring the novel object or location and the average time spent exploring the familiar object or location expressed as a percentage of the total time spent exploring during the test phase.

Immunoblotting

Half brain cortical tissue and hippocampi were homogenized in T-PER buffer with protease and phosphatase inhibitor cocktails (ThermoFisher). Protein extract was then centrifuged at 100 000 × g for 1 h at 4°C, and supernatant was taken as the detergent soluble fraction. The pellet was resuspended in 88% formic acid and centrifuged again at 100 000 × g for 1 h at 4°C and the supernatant from this step was taken as the formic acid soluble fraction.

For the vascular enriched protein samples, half brains were homogenized in sucrose buffer (0.32 M sucrose, 3 mM HEPES, Fisher) using a glass Dounce homogenizer. Samples were centrifuged at 1000 × g for 10 min at 4°C. This process was repeated for the resultant pellet. The pellet was then rehomogenized and centrifuged at 100 × g for 30 s; the resulting supernatant was stored and this process repeated once. The supernatant fractions of the vascular enriched protein samples were pooled and spun for 2 min at 200 × g, and the final pellet was resuspended in 0.1% BSA (ThermoFisher) as the vascular enriched protein fraction. Protein concentration was determined by the Bradford protein assay. Protein samples were run on Bio-Rad Mini-PROTEAN TGX gels (Bio-Rad Laboratories) at 150 V and transferred to Immobilon-FL PVDF membranes (Millipore-Sigma). After 1 h blocking in Li-Cor Odyssey Blocking Buffer in tris-buffered saline (TBS) (Li-Cor Biosciences), membranes were immunoblotted with

the following antibodies overnight at 4°C: Glyceraldehyde-3-phosphate dehydrogenase (GAPDH, 1:1000, Santa Cruz Biotechnology), tubulin (Tub, 1:25 000 Abcam), postsynaptic density protein 95 kDa (PSD95, 1:1000, Cell Signaling Technology), synaptophysin (SYP, 1:1000, Cell Signaling Technology), glial fibrillary acidic protein (GFAP, 1:1000, DAKO), Iba1 (1:1000, Fujifilm Wako), and amyloid precursor protein, c-terminal (751–770) (CT-20, 1:1000, Millipore-Sigma). Membranes were then washed, incubated for 1 h at room temperature with secondary antibodies Goat anti Rabbit or Goat anti Mouse IRDye 680 and 800 (1:20 000 Li-Cir Biosciences), washed again and read. Blots were read using the Li-Cor Odyssey system and Image Studio software version 5 (Li-Cor Biosciences) to obtain band signal intensity. Signal is expressed relative to tubulin or GAPDH levels, which were used for protein loading controls before statistical analysis.

Immunostaining

Another brain hemisphere from each animal was fixed with 4% paraformaldehyde, cryoprotected in 30% sucrose solution, and stored in –80°C. Fixed brain hemispheres were then sectioned into 40 µm slices coronally using a microtome and stored in phosphate buffered saline with 0.05% sodium azide. Sections were mounted on standard glass microscope slides (Fisher) before staining. For antibody staining sections were permeabilized with 0.1% Triton X-100 in TBS for 15 min and blocked with 3% bovine serum albumin (Fisher), 5% normal goat serum (Vector Laboratories), and 0.1% Triton X-100 in TBS for 1 h. For amyloid-β (Aβ) plaque staining sections were treated with 70% formic acid for 5 min before other treatments. After pretreatment and blocking, the sections were incubated with primary antibodies against NeuN (1:5000, Abcam), PSD95 (1:1000, Cell Signaling Technology), synaptophysin (1:1000, Cell Signaling Technology), GFAP (1:1000, DAKO), Iba1 (1:1000, Abcam), C3 (1:3000, HyCult), Tmem119 (1:5000, Abcam), ferritin (1:5000, Millipore-Sigma), or anti-Aβ 82E1, whose epitope is Aβ N-terminal (1:1000, Immuno-Biological Laboratories) overnight at 4°C. Sections were washed with TBS and treated for 1 h at room temperature the following day in 3% BSA, 5% normal goat serum, and 0.1% Triton X-100 in TBS with secondary antibodies conjugated with Alexa Fluor 488, 555, or 633 (Fisher). For Thioflavin S staining, brain sections were rehydrated with ethanol at 100%, 95%, 70%, and 50% and then treated with Thioflavin S (Millipore-Sigma) in 50% ethanol for 10 min. Slides were mounted with Fluoromount-G (Fisher). For Nissl staining, mounted brain sections were first incubated in 1:1 mixture of ethanol and chloroform overnight, followed by 0.1% cresyl violet solution for 10 min. Images were taken with either a Leica TCS SPE confocal microscope or Keyence BZ-X800 fluorescence/phase-contrast microscope. Images from all stained sections (1–2 sections/animal) were taken using Keyence BZ-X800 fluorescence/phase-contrast microscope or Leica TCS SPE confocal microscope and with 10–40× objective. The immuno-positive (82E1, Iba1, Tmem119, Ferritin and GFAP) or Thioflavin-S-positive areas were analyzed both in the hippocampus and cortex between Bregma coordinates –1.58 and –1.82 mm. These images were processed using the ImageJ 1.52p image analysis system. The 24-bit color digital images were calibrated (scale bar of 400 µm = 520 pixels; 1.300 pixels/µm) and transformed to grayscale images (8-bits). After manually delimiting the reference area (excluding tissue ruptures, large blood vessels, or white matter areas), images were binarized using a threshold level mask that was fixed between a range of 170–180 of intensity and manually set for each image to ensure a reliable quantification. The coverage area within the region of interest was estimated and

defined as sum labeled area measured/sum total area analyzed. All slides sampled were taken over for the sums, and a single burden was computed for each individual. The mean and standard deviation (SD) of the corresponding loadings were determined using all available data. To make accurate comparison between study groups tissue samples and sections were simultaneously processed using standardized handling and immunostaining protocols. For GFAP/C3 staining, all images were captured by 10× objective, and the number of GFAP+/C3+ cells, GFAP+/C3– cells, and GFAP+ cells (85–196 counts) were counted within the defined area in the cortex. For NeuN and Nissl staining, we counted the number of NeuN- or Nissl-positive cells in the defined area and expressed as positive cell counts per millimeter square.

qPCR analysis

RNA was isolated from *App*^{NL-G-F/+}-KI mouse hippocampal and cortical brain tissue in TRI reagent and extracted using the Direct-Zol RNA MiniPrep kit (ZYMO Research Corp) used according to the manufacturer's instructions. RNA concentration in the extract was quantified using a NanoDrop Lite (ThermoFisher). One microgram of total RNA was used in a single cycle reverse transcriptase reaction of 5 min at 25°C, 20 min at 46°C, 1 min at 95°C to make cDNA using iScript reaction mix and reverse transcriptase (Bio-Rad Laboratories). Two microliters of cDNA were used per reaction using iTaq Universal SYBR Green Supermix (Bio-Rad Laboratories) for detection of *Il1β*, *Il6*, and *App*. Expression levels were normalized with *Gapdh* mRNA levels. Primer sequences are as follows: *Il1β* forward 5'-TGGACCTTCCAGGATGAGGACA-3' reverse 5'-GTTTCATCTCGGAGCCTGTAGTG-3' (Origene NM_008361), *Il6* forward 5'-TACCACCTTCAACAAGTCGGAGGC-3' reverse 5'-CTGCAAGTGCATCATCGTTGTTC-3' (Origene NM_031168), *Gapdh* forward 5'-AACTT TGGCATTGTGGAAGG-3' reverse 5'-ACACATTGGGGGTAGGAAC A-3' (Origene NM_010277), *App* 5'-TCCGTGTGATCTACGAGCGCA T-3' reverse 5'-GCCAAGACATCGTCGGAGTAGT-3' (Origene NM_007471). The PCR cycle parameters are listed: denaturing step (95°C for 15 s), annealing step (60°C for 60 s), and extension step (72°C for 30 s). Bio-Rad CFX Manager software version 3.1 was used to determine Cq values. ΔCq values were determined as determined by the difference between the gene of interest Cq and *Gapdh* Cq. ΔCq values between filtered air exposed and PM exposed animals were compared with obtain relative expression values, with the filtered air group set to 1.

Aβ assay

Detergent soluble and formic acid soluble Aβ_{1–40} and Aβ_{1–42} levels were measured using the V-PLEX Aβ Peptide Panel with 6E10 capture antibody used as recommended by the manufacturer and read on a MESO QuickPlex SQ 120 (Meso Scale Discovery) for the 6-month group. For the 9- and 12-month groups Aβ levels were quantified using Human βAmyloid (1–40) ELISA kit and Human βAmyloid (1–42) ELISA kit (Fujifilm Wako). Protein sample extracts were obtained and quantified as described under protein extraction and Western blots. One hundred microliters of protein were loaded per well for each sample. Bradford protein assay concentration readings were used to adjust for total protein loaded per sample.

Statistical analysis

Immunoblots were quantified using Image Studio Software version 5. Immunofluorescent images were quantified using ImageJ version 1.52. All other data were analyzed using Microsoft Excel (Microsoft Office 365 ProPlus) or Prism version 9 (GraphPad

Software). Statistics were conducted using unpaired *t* test (to compare 2 groups), one-way analysis of variance (ANOVA) with Tukey's post hoc test (to compare more than 2 groups) or two-way ANOVA with Tukey's post hoc test (to compare groups with 2 independent variables). *p*-Values $\leq .05$ were considered significant. Sex differences were generally not observed, partly due to low numbers of animals between males and females, and data are presented as mixed groups.

Results

Characterization of concentrated ambient particles by VACES

Particulate matter sources at the Irvine site are predominantly motor vehicle emissions from freeways and nearby roads, construction and light industry and regional background. At our site, 90% of PM are diameter $<2.5\mu\text{m}$, and ultrafine PM represents over 50% of all PM counts. The average concentration of PM (diameter $<180\text{nm}$) by VACES for 3–6 months study (performed in August–November 2017) or 9–12 months study (performed in February–April 2019) was approximately 70 000 or 130 000 particles/cm³ (p/cm³) over the entire exposure period, respectively, which was approximately 7–8 times more concentrated than average ambient PM levels over the same time period (Figure 1B). Particle numbers within the purified air controls were consistently low and averaged 3.0 ± 0.9 p/cm³ over the entire exposure period. Similarly, the average particle mass concentration of PM delivered by the VACES was $108.9\mu\text{g}/\text{m}^3$ (3–6 months study) or $84.8\mu\text{g}/\text{m}^3$ (9–12 months study) during the exposure period, which was approximately 4–6 times more concentrated than the average ambient particle mass concentrations (Figure 1C). Particle masses measured in the purified air controls was averaged $1.2\mu\text{g}/\text{m}^3$ over the course of the exposure.

Exposure to concentrated PM impairs cognition without overt exacerbation of AD neuropathology in young, prepathological *App*^{NL-G-F/+}-KI mice

At the end of exposure, all mice were subject to OLM followed by ORM tasks to assess hippocampus-based spatial memory and cortical-dependent recognition memory, respectively. Three-month-old heterozygous *App*^{NL-G-F/+}-KI mice (mixed sex, *n* = 12 per group) exposed to PM were significantly impaired in both

memory tasks compared with filtered air exposed mice (Figs. 2A and 2B).

In AD, cognitive decline and memory impairment are strongly associated with extensive loss of synapses and neurons. Synapse and neuronal density changes were examined in the cortex and hippocampal regions. Changes in synapse density were visualized using PSD95 and synaptophysin staining while in neuronal density changes were visualized using NeuN and Nissl staining. Mean intensities of PSD95 and synaptophysin in both hippocampus and cortex were not different between filtered air and PM exposed *App*^{NL-G-F/+}-KI mice (Figure 3A). These results were also confirmed by immunoblot of PSD95 and synaptophysin (Figure 3B). Likewise, no significant difference was observed in NeuN or Nissl staining (data not shown). Therefore, cognitive impairment detected in PM-exposed *App*^{NL-G-F/+}-KI mice at this stage was not caused by a clear synapse or neuronal loss in either brain region.

We next examined whether development of AD-related neuropathology was accelerated following PM exposure. *App*^{NL-G-F/+}-KI mice at this age start to develop plaque pathology mainly in the cortex but is virtually absent in the hippocampus (Saito et al., 2014). No significant differences in overall 82E1-positive A β plaque burden by immunostaining and A β 42 levels by ELISA between the control and PM exposure group were observed in the cortex or hippocampal regions (Figure 4A). Furthermore, APP expression was not altered by PM exposure as the steady-state levels of full-length APP, detected by CT20 antibody, or *App* mRNA were unchanged between the exposures (Figs. 4B and 4C). Glial activation detected by Iba1 and GFAP immunoreactivity and mRNA expression was not different between the control and PM exposure groups (Figs. 5A–C) (Patten et al., 2021).

PM exposure impairs cognition in aged wildtype and *App*^{NL-G-F/+}-KI mice

Nine-month-old *App*^{NL-G-F/+}-KI mice and their littermate WT counterparts were exposed to concentrated PM for 12 weeks in the same fashion as the PM exposure with 3-month-old old animals. This advanced-age exposure paradigm could simulate a late-life exposure to PM in humans, which is considered to take account for up to 2% of the estimated risk for dementia from suspected modifiable risk factors (Livingston et al., 2020). We found that PM exposure significantly impaired memory function

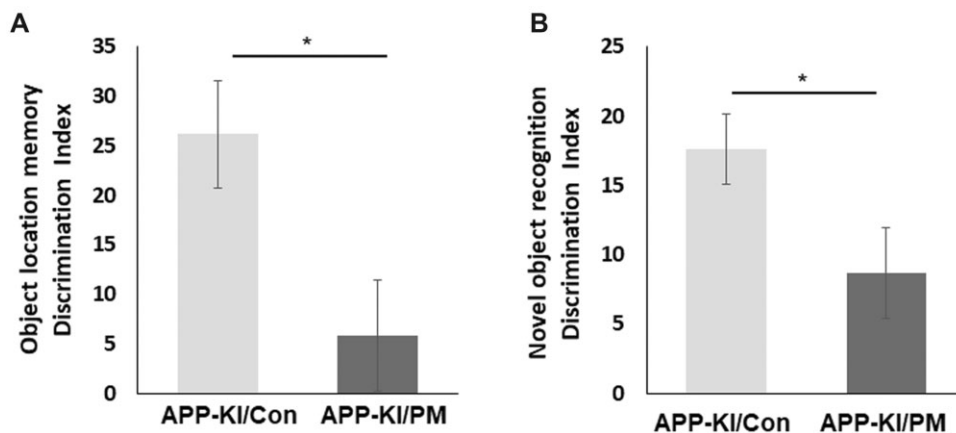


Figure 2. Particulate matter exposure impairs memory performance in young, prepathological *App*^{NL-G-F/+}-KI mice. A battery of cognitive tests was initiated 3 weeks before the end of 12-week PM exposure as indicated in Figure 1A. Six months old *App*^{NL-G-F/+}-KI mice (*n* = 12 per group, mixed sex) underwent OLM testing (A) followed by ORM testing (B). A reduced discrimination index indicates memory impairment. Bars represent mean values, with error bars expressed as standard error of the mean (**p* < .05). Con, filtered air control group; PM, concentrated quasi-ultrafine PM exposed group.

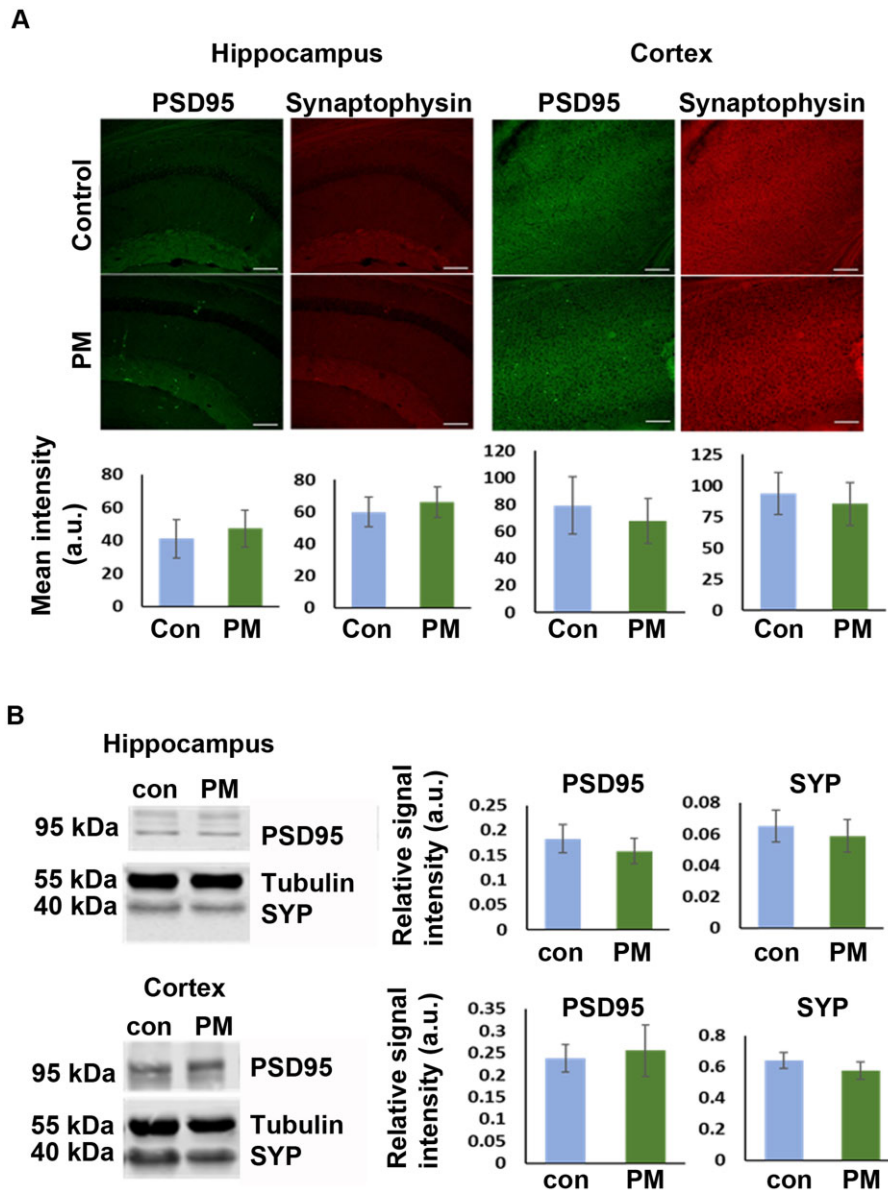


Figure 3. Particulate matter exposure does not induce changes in synaptic markers in young *App*^{NL-G-F/+}-KI mice. A, Representative images of PSD95 and synaptophysin immunofluorescent staining with fluorescent intensity quantification for the CA1 region of the hippocampus (left) and the cortex (right). B, Representative immunoblot bands of PSD95 and synaptophysin (SYP) in soluble homogenate tissue extracts from the hippocampus (left) and the whole cortex (right). Tubulin was used as a house-keeping protein to normalize band intensity. Graphs show normalized relative band intensity of PSD95 and SYP. Bars represent mean values with error bars expressed as standard error of the mean ($n = 8$ per group for immunostaining and $n = 10$ per group for immunoblot. Scale bars = 100 μ m).

particularly in WT mice. Although the significant difference (approximately 58% decrease in discrimination index, $p < .01$) was found only between the filtered air-exposed WT and PM-exposed *App*^{NL-G-F/+}-KI mice in OLM, the discrimination index for ORM was decreased by approximately 38% ($p = .0361$) with PM exposure within the WT mice and by approximately 61% ($p = .0504$) with PM exposure within the *App*^{NL-G-F/+}-KI mice (Figure 6A). Although the reduction of discrimination index was greater in *App*^{NL-G-F/+}-KI mice, it did not achieve a significance, partly because a significant genotype-dependent impairment of recognition memory in *App*^{NL-G-F/+}-KI mice at 12 months of age lowered its baseline (control) discrimination index. Such genotype-dependent cognitive impairment was well-documented in *App*^{NL-G-F}-KI mice with increasing age (Latif-Hernandez et al., 2019; Masuda et al., 2016; Mehla et al., 2019).

Impaired cognitive function in both WT and *App*^{NL-G-F/+}-KI mice following PM exposure indicated that it might, in part, be mediated independently by A β pathology. An analysis of neuronal density using NeuN and Nissl staining found a significant difference neurons between filtered air- and PM-exposed *App*^{NL-G-F/+}-KI mice in the entorhinal cortex; no difference in the number of NeuN- or Nissl-positive neurons was detected in the CA1 hippocampus among the 4 groups (Figs. 6B and 6C; Supplementary Figure 1).

PM exposure heightens A β plaque burden in aged *App*^{NL-G-F/+}-KI mice

The A β plaque pathology in aged *App*^{NL-G-F/+}-KI mice was evaluated. The PM exposure significantly exacerbated Thioflavin S-positive dense core plaques in both cortex (0.48% compared with

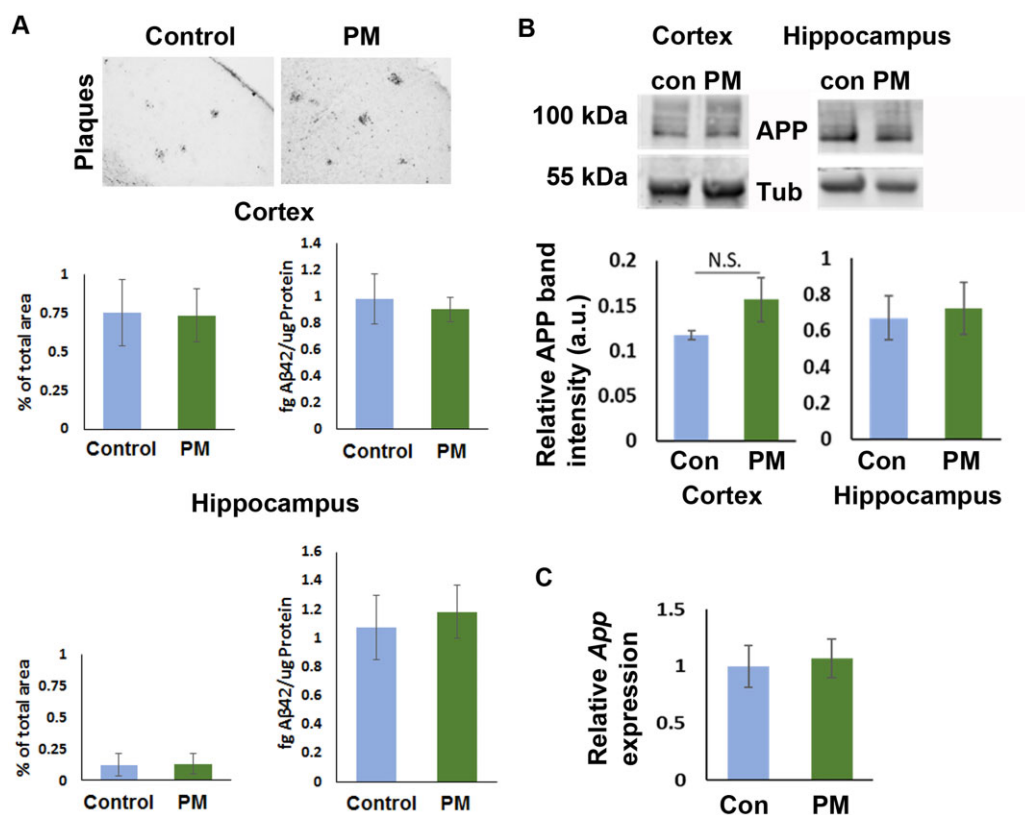


Figure 4. Particulate matter exposure does not exacerbate A β plaque burden in young *App*^{NL-G-F/+}-KI mice. A, Brain sections were stained with 82E1 antibody to detect A β plaques in *App*^{NL-G-F/+}-KI mice. Representative images of cortical A β plaque burden from the parietal cortex in *App*^{NL-G-F/+}-KI mice exposed to filtered air (control, left) and PM (right) are shown. Quantification of A β plaque burden was calculated and expressed as percentage of the total measured area occupied by 82E1-positive plaques in the cortex and the hippocampus (graphs on left, $n = 8$ per group). Soluble A β 42 in the cortical and the hippocampal tissues was quantified by MSD and expressed in fg/ μ g protein (graphs on right, $n = 6$ per group). B, Steady-state levels of full-length APP in the cortical or hippocampal tissues were detected by immunoblot using CT20 antibody. Relative band intensity for APP was normalized with tubulin band intensity throughout the samples and expressed in the graph ($n = 6$ per group). C, *App* mRNA expression in the cortical tissue was normalized to *Gapdh* mRNA and expressed in the graph ($n = 6$ per group).

0.83% of total area, $p < .01$) and hippocampus (0.26% compared with 0.59%, $p < .05$), whereas 82E1-positive A β plaques (staining both diffused and dense core) were only significantly increased in the cortex of PM-exposed *App*^{NL-G-F/+}-KI mice (2.2% versus 1.4%, $p < .01$, Figure 7A). Consistent with young *App*^{NL-G-F/+}-KI cohorts, no significant difference was observed in the steady-state levels of full-length APP or *App* mRNA (Figs. 7B and 7C).

Glial activation was exacerbated in exposure- and genotype-dependent manners

Microglia and astrocyte activation were assessed because PM-induced glial or inflammatory activation is one of prominent feature in the brain (Bhatt et al., 2015; Calderon-Garciduenas et al., 2004; Campbell et al., 2005, 2009) and could mediate neurodegeneration. Overall microglial activation was first assessed by quantifying the Iba1-positive area in the cortex and the hippocampus. A significant, genotype-dependent, increase of Iba1-positive microglia was measured in *App*^{NL-G-F/+}-KI mice over WT mice primarily due to the presence of A β plaques (Figure 8A). In addition, Iba1-positive microglia were significantly increased in an exposure-dependent manner between the PM-exposed *App*^{NL-G-F/+}-KI mice when compared with filtered air-exposed *App*^{NL-G-F/+}-KI mice (Figure 8A). This was not, however, observed in WT mice. No significant increase of Iba1-positive microglia was found in the hippocampus from any of the 4 exposure groups.

Distinguishing harmful microglia subpopulations by transcriptomics in this study was not feasible. Therefore, homeostatic Tmem119-positive microglia (Bonham et al., 2019; Butovsky et al., 2014; Satoh et al., 2016) and highly activated, potentially degenerative ferritin-positive microglia (Kenkhuis et al., 2021; Meng et al., 2017; Reinert et al., 2019) were identified in the brain to predict the prevalence of potentially harmful microglia following PM exposure. Compared with Iba1 staining, which stained all microglia population in the brain, Tmem119-positive microglia were predominantly identified in ramified morphology and absent around A β plaques while ferritin-positive microglia were predominantly found around plaques (Supplementary Figure 2). Tmem119-positive microglia found vicinity in the of 82E1-positive plaques in *App*^{NL-G-F/+}-KI mice were not significantly different between the exposures (Figure 8B). However, nonplaque associated Tmem119-positive microglia were significantly reduced in PM-exposed mice (both WT and *App*^{NL-G-F/+}-KI mice). Likewise, ferritin-positive microglia were increased in the cortex and the hippocampus of PM-exposed *App*^{NL-G-F/+}-KI mice compared with filtered air control group (Figure 8C). This was due to increased A β plaque burden. No cluster of ferritin-positive microglia was detected in WT mice, primarily because of the absence of plaques (Figure 8C). On the other hand, ferritin+ clusters were present in *App*^{NL-G-F/+}-KI mice, and its distribution pattern was quite similar to A β plaques, indicating that these are clusters of activated microglia around plaques.

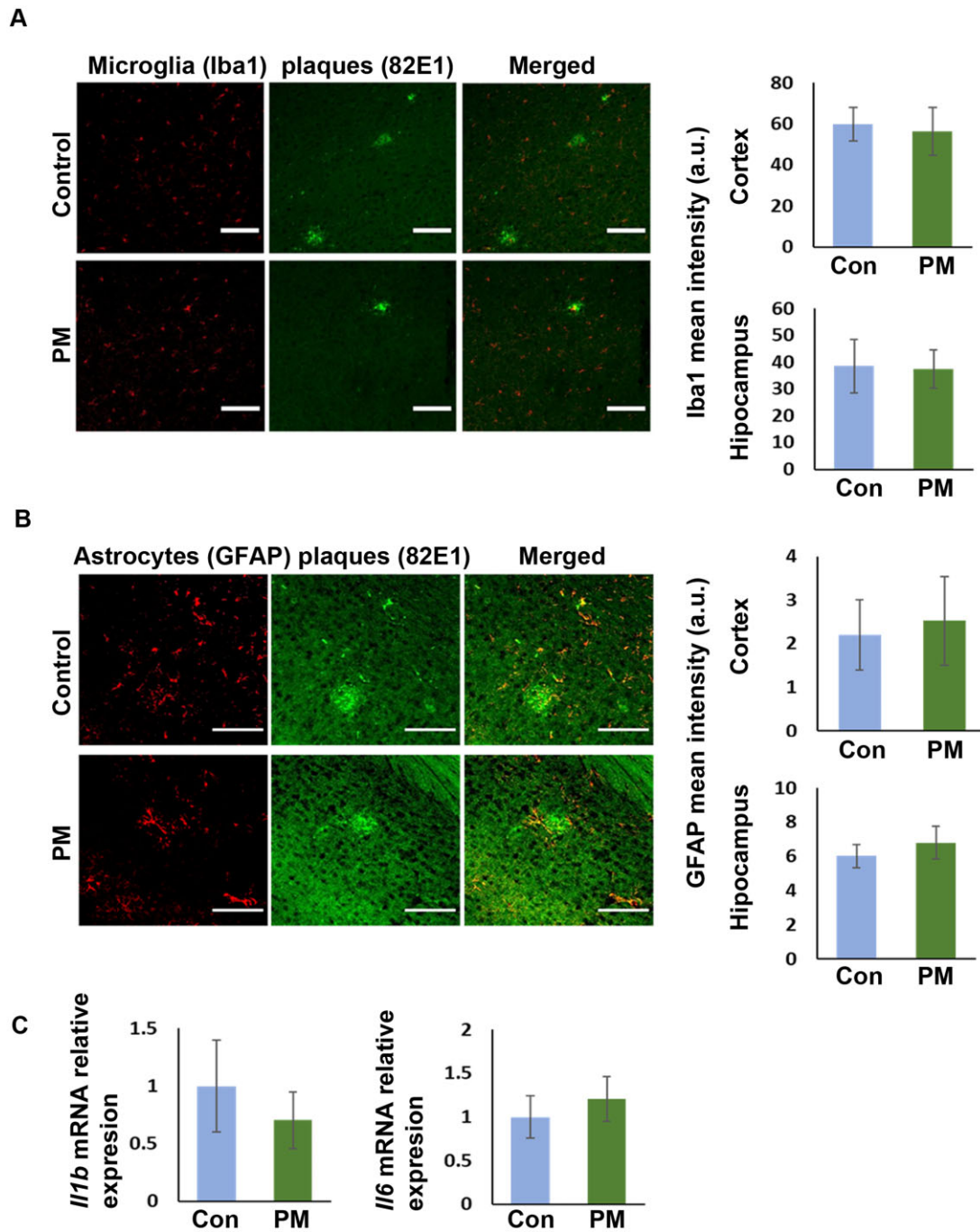


Figure 5. Glial activation was not altered in PM-exposed young $App^{NL-G-F/+}$ -KI mice. A, Representative images of microglial marker Iba1 and A β (82E1) staining taken from the parietal cortex. Signal intensity was quantified and expressed in the graphs as the mean fluorescent intensity of Iba1 in the cortex and the hippocampus, respectively ($n = 8$ per group, scale bars = 100 μ m). B, Representative images of astrocytic marker GFAP and A β (82E1) staining taken from the parietal cortex. Signal intensity was quantified and expressed in the graphs as the mean fluorescent intensity of GFAP in the cortex and the hippocampus, respectively ($n = 8$ per group, scale bars = 100 μ m). C, mRNA expressions of pro-inflammatory cytokines *Il1 β* and *Il6* in the cortical tissue were normalized to *Gapdh* mRNA. Neither *Il1 β* nor *Il6* mRNA levels were significantly affected by the exposure status ($n = 6$ per group).

However, ferritin⁺ area was found to be increased in PM-exposed $App^{NL-G-F/+}$ -KI mice when compared with control $App^{NL-G-F/+}$ -KI mice, but it was not statistically significant (Figure 8C, top graph). Intriguingly, we found ferritin-positive microglia-like single cells in the cortex and the hippocampus away from plaques in both WT and $App^{NL-G-F/+}$ -KI mice (Figure 8C, arrows). The number of ferritin-positive single cells were significantly increased by PM exposure in both genotypes (Figure 8C, bottom

graph). Together, a clear shift from Tmem119-positive microglia to ferritin-positive microglia following PM exposure could lead to more neurodegenerative microenvironment in the brain of these animals.

Lastly, we measured GFAP-positive astrocytes and the extent of gliosis in the brain. The number of astrocytes and gliosis were significantly increased in the cortex, but not in the hippocampus, of $App^{NL-G-F/+}$ -KI mice over WT mice, regardless of exposure

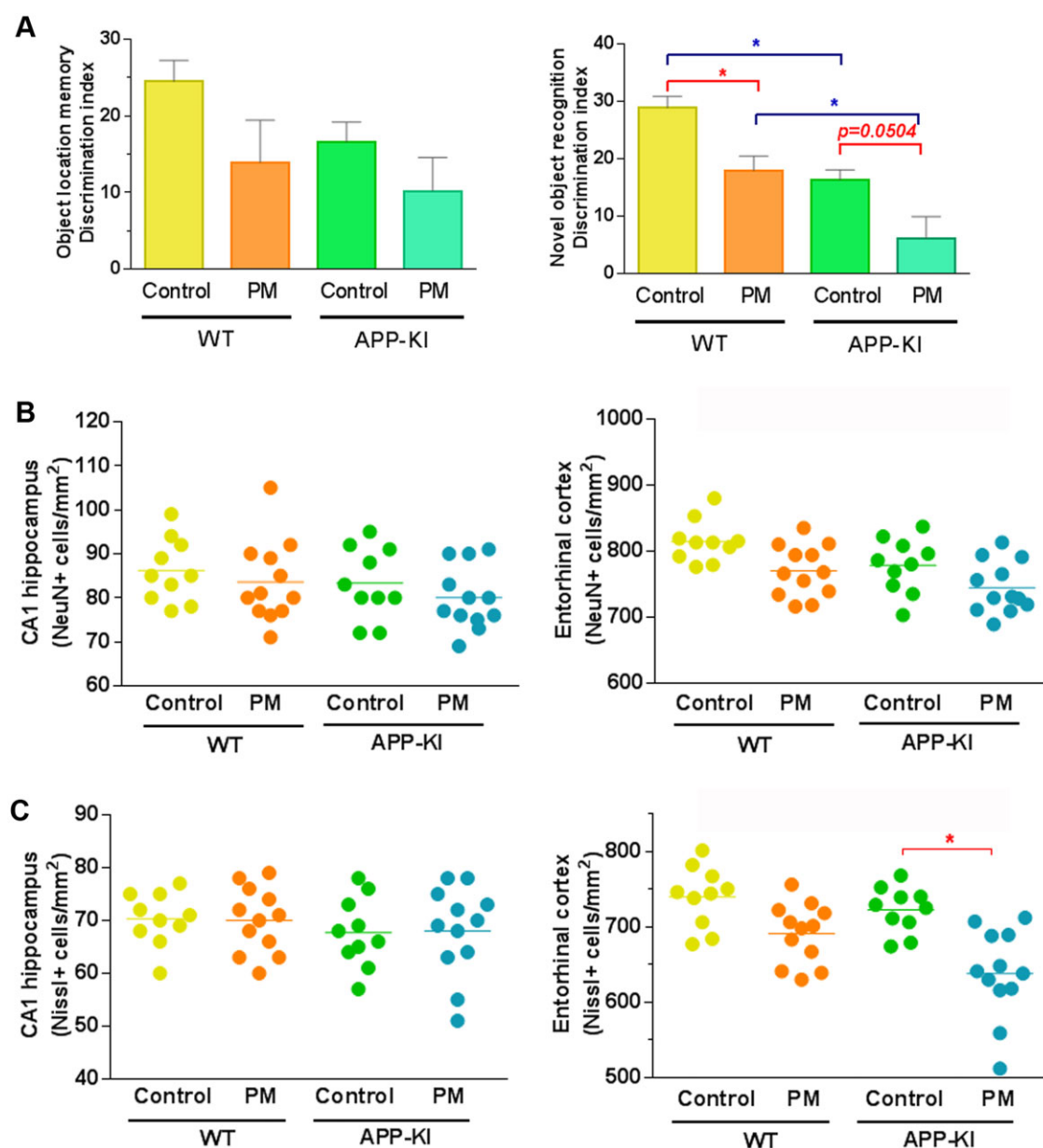


Figure 6. Particulate matter exposure accelerates memory impairment and neuronal loss in older WT and *App^{NL-G-F/+}-KI* mice. A, All WT and *App^{NL-G-F/+}-KI* mice ($n = 12$ per group, mixed sex) underwent OLM (left), followed by ORM (right) testing starting 3 weeks prior to the end of 12-week PM exposure. A reduced discrimination index indicates memory impairment by each test. Bars represent mean values with error bars expressed as standard error of the mean. Blue lines and asterisks indicate genotype-dependent differences (WT vs *App^{NL-G-F/+}-KI*), and red lines and asterisks indicate exposure-dependent differences (filtered air vs PM exposure) detected between the two groups ($p < .05$). B, Graphs represent the number of NeuN+ neurons in the CA1 hippocampus (left) and entorhinal cortex (right). C, Graphs represent the number of neurons by Nissl staining in the CA1 hippocampus (left) and entorhinal cortex (right). Each NeuN and Nissl staining was performed in 2 separate brain sections per animal. Red line and asterisk indicate an exposure-dependent change in the neuronal counts ($n = 5-6$ animals per group, $*p < .05$).

(Figure 9A; Supplementary Figure 3). Since the number of GFAP-positive astrocytes do not accurately reflect their activation status, we used C3 to estimate the abundance of neurotoxic astrocytes in mice exposed to PM based on recent reports unveiling neurotoxic activation of astrocytes (Bonham et al., 2019; Butovsky et al., 2014; Liddelow et al., 2017; Mathys et al., 2019; Spangenberg et al., 2019; Wu et al., 2019; Zamanian et al., 2012). C3+/GFAP+ neurotoxic astrocytes in cortex were significantly increased in PM-exposed WT and *App^{NL-G-F/+}-KI* mice when compared with filtered air-exposed group within the same genotype (Figure 9B), indicating potential involvement of harmful neuroinflammation elicited by PM exposure in neuronal death and functional decline.

Discussion

We report that exposure to concentrated PM was associated with decreased performance in both the cortical-dependent recognition memory and the hippocampus-dependent spatial memory in young *App^{NL-G-F/+}-KI* mice while preferentially impairing recognition memory in older WT and *App^{NL-G-F/+}-KI* mice. These results are consistent with previous reports showing accelerated cognitive decline in animals exposed to PM (Fonken et al., 2011; Jew et al., 2019; Patten et al., 2021) and further supports epidemiologic studies showing detrimental effects of air pollution on one's cognitive capacity (Cacciottolo et al.,

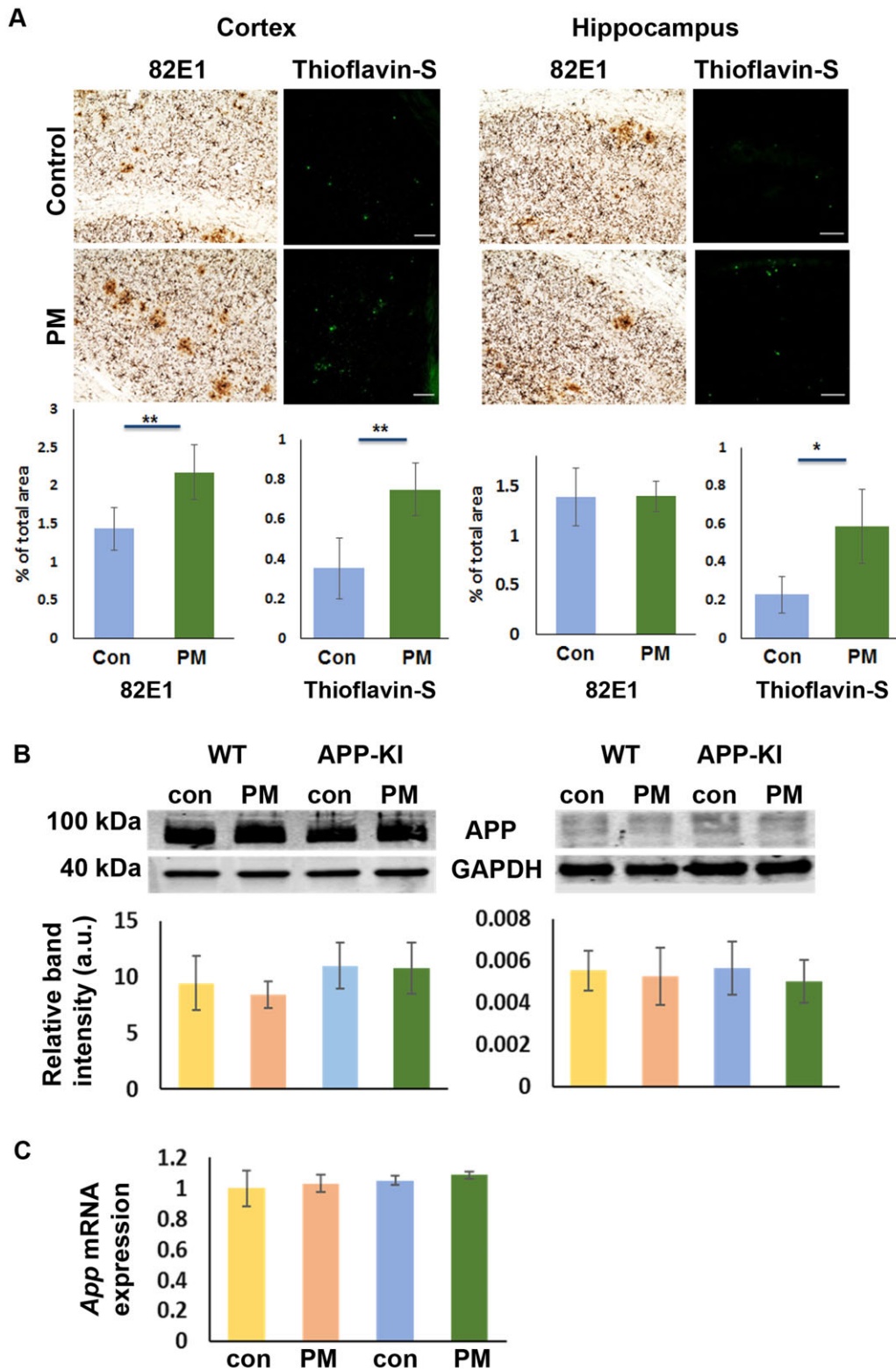


Figure 7. Amyloid- β plaque burden is exacerbated by PM exposure in old *App*^{NL-G-F/+}-KI mice. Brain sections were stained with 82E1 antibody and Thioflavin S to detect diffuse and dense core A β plaques in *App*^{NL-G-F/+}-KI mice. A, Representative images of A β plaque burden detected by 82E1 antibody and Thioflavin S from the parietal cortex (left) and CA1 region of the hippocampus (right) in *App*^{NL-G-F/+}-KI mice exposed to filtered air or PM. Quantification of plaque burden by these 2 stained images is expressed as the percentage of the total measured area occupied by plaques (n = 6 per group, scale bars = 100 μ m, *p < .05 or **p < .01). B, Steady-state levels of full-length APP in the cortical or hippocampal tissue were detected by immunoblots and expressed as the mean \pm S.E.M with band intensity normalized using GAPDH (n = 4 per group). C, *App* mRNA expression in the cortex was measured by qPCR and normalized with *Gapdh* mRNA (n = 4 per group).

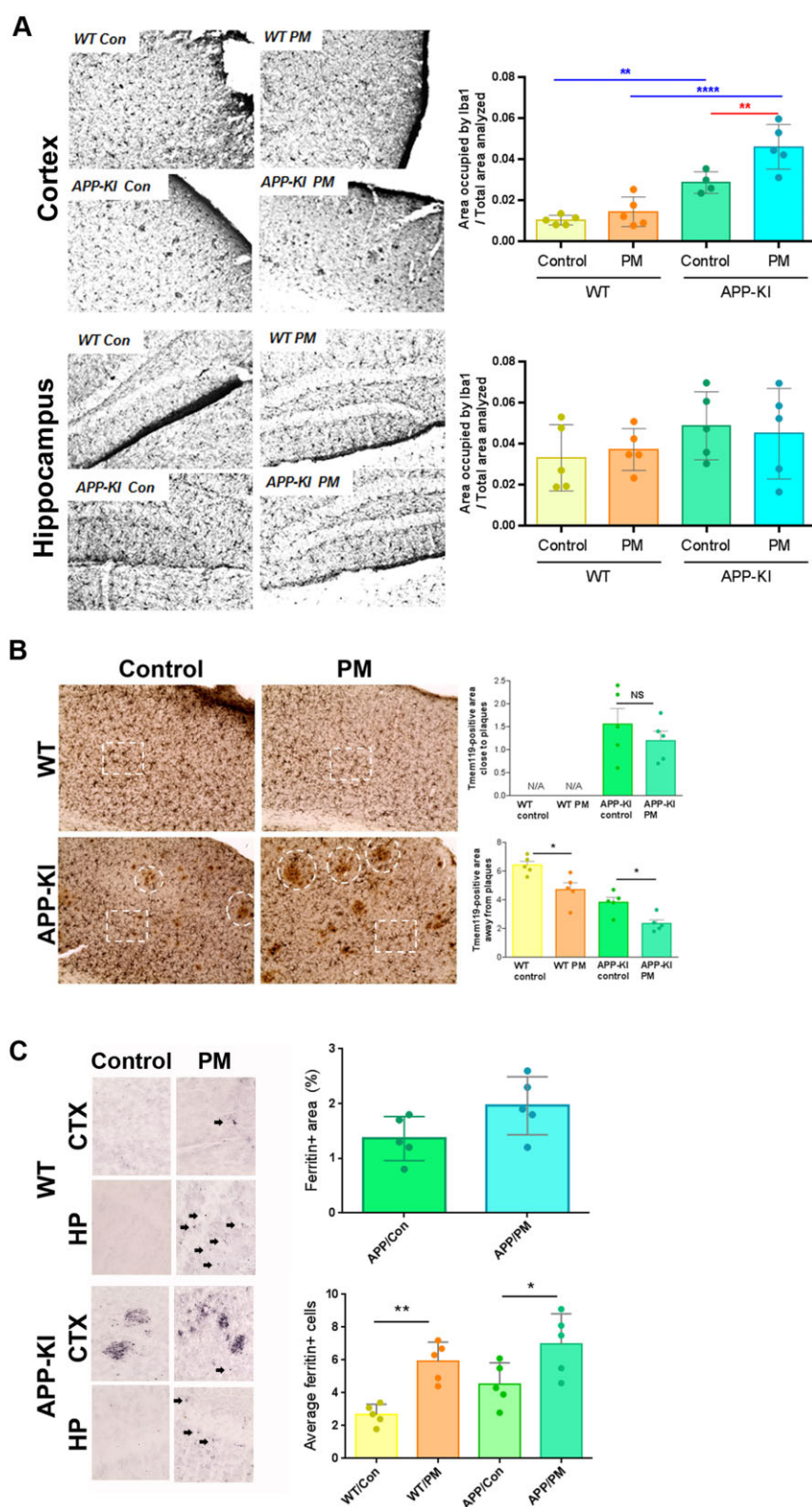


Figure 8. Degenerative microglia activation is increased by PM exposure in both WT and *App^{NL-G-F/+}*-KI mice. **A**, Brain sections were stained with Iba1 antibody to detect microglia. Area covered by Iba1 staining was quantified in the cortex (left) and the hippocampus (right) separately and compared among the groups. Graphs represent the mean \pm S.E.M. ($n = 5$ per group). Blue lines and asterisks indicate genotype-dependent differences (WT vs *App^{NL-G-F/+}*-KI) while red lines and asterisks indicate exposure-dependent differences (filtered air vs PM exposure) detected between the 2 groups (** $p < .01$, **** $p < .0001$). **B**, Brain sections were costained with Tmem119 (dark blue/black) and A β plaques (82E1 antibody, brown). Tmem119+ microglia were analyzed around plaques (ie, dotted circle, top graph) or away from plaques (ie, dotted square, bottom graph) in the cortex. Graphs represent the mean \pm S.E.M ($n = 5-6$ per group, * $p < .05$). **C**, Area covered by ferritin+ microglia were quantified in the brain of *App^{NL-G-F/+}*-KI mice ($n = 5$ per group). Arrows in magnified images indicate representative ferritin-positive microglia-like single cells in each group. Top graph shows area covered by ferritin-positive staining in both the cortex and the hippocampus, and bottom graph shows the average number of ferritin-positive single cells in the cortex and hippocampus of each group ($n = 5$ per group, * $p < .05$, ** $p < .01$ between the indicated groups).

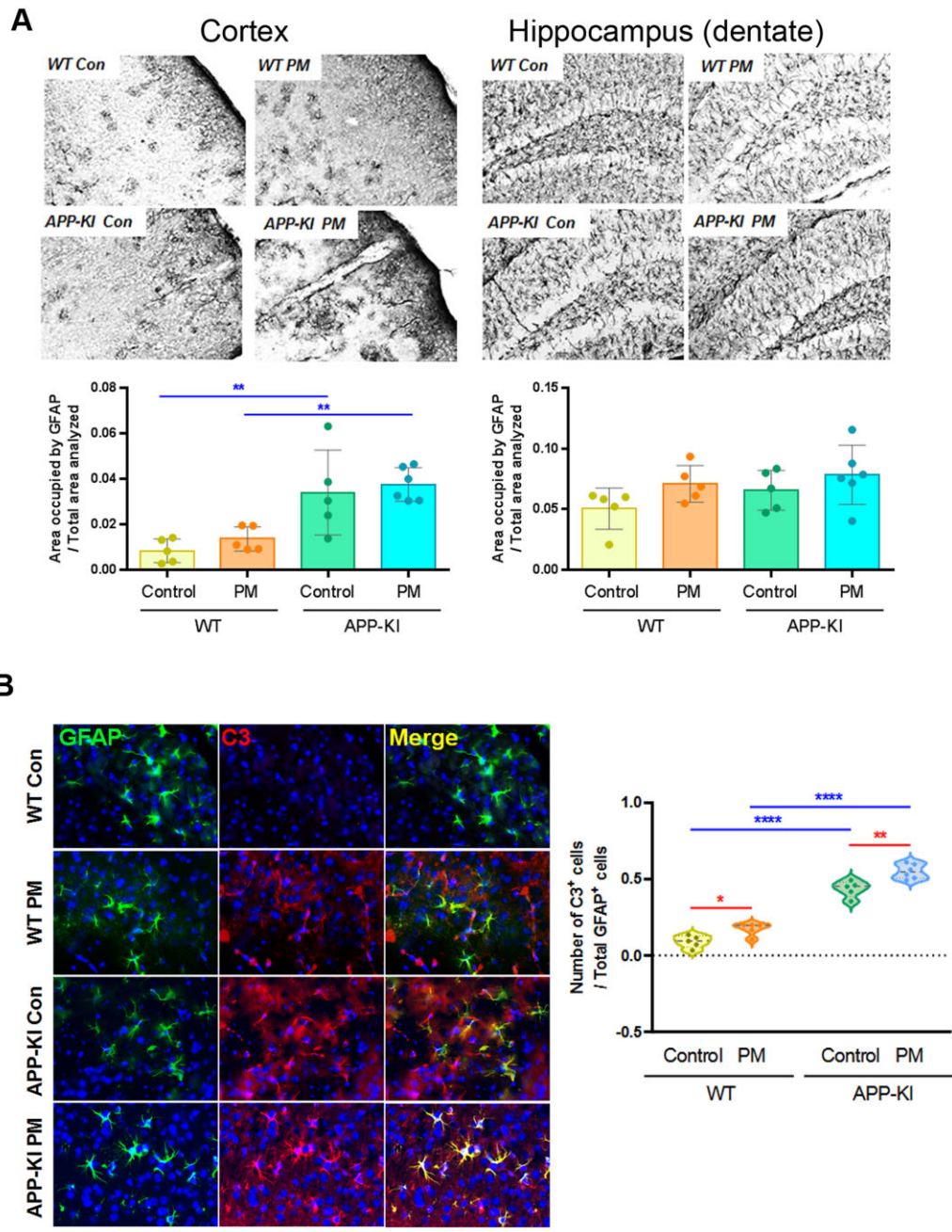


Figure 9. Neurotoxic astrocyte activation is exacerbated by PM exposure in *App^{NL-G-F/+}-KI* mice. A, Brain sections were stained with GFAP antibody to detect astrocytes. Area covered by GFAP staining was quantified in the cortex (left) and the hippocampus (right) separately and compared among the groups. Graphs represent the mean ± S.E.M. (*n* = 5–6 per group). Blue lines and asterisks indicate genotype-dependent differences (WT vs *App^{NL-G-F/+}-KI*). ***p* < .01 between the indicated groups. B, Brain sections were costained with GFAP and C3, and nuclei were stained with DAPI. Double positive GFAP+/C3+ astrocytes in the cortex were counted and expressed as percent of total GFAP+ cell counts in the graph. Blue lines and asterisks indicate genotype-dependent differences (WT vs *App^{NL-G-F/+}-KI*) while red lines and asterisks indicate exposure-dependent differences (filtered air vs PM exposure) detected between the 2 groups (**p* < .05, ***p* < .01, *****p* < .0001).

2017; Carey et al., 2018; Harris et al., 2015; Jedrychowski et al., 2015; Lin et al., 2017; Shi et al., 2020; Weuve et al., 2012; Zhang et al., 2018). We show that 12-week PM exposure exacerbated AD-related neuropathology, neuronal loss, and glial activation when animals were exposed at a later age. Potentially harmful transformation and activation of microglia and astrocytes, as indicated by reduced Tmem119 and increased ferritin immunoreactivity in microglia and increased C3 immunoreactivity in astrocytes, was promoted by PM exposure. Such detrimental shift of glial activation in the brain may be one of the key

underlying neurotoxic mechanisms elicited by PM and accelerate the progression of AD phenotypes.

Our current findings add several notable features of PM neurotoxicity relevant to AD. First, increased Aβ plaque burden in old *App^{NL-G-F/+}-KI* mice following PM exposure is not only consistent with previous reports in different rodent transgenic models (Bhatt et al., 2015; Cacciottolo et al., 2017; Patten et al., 2021) but also validates knowledge that PM exposure exacerbates plaque development even in brains physiologically expressing APP and advancing age and pathology may be critically contributing to

such change triggered by the environmental risk factor. Increased A β deposits in PM-exposed *App*^{NL-G-F/+}-KI mice are unlikely mediated by elevated expression of *App* in the brain as the steady-state levels of full-length APP and *App* mRNA levels remain unaltered by the exposure. However, the absence of increased A β pathology following exposure to concentrated PM in young, prepathologic mice as well as memory impairments in WT animals in the aged group suggests that the mechanisms by which PM exposure impairs cognitive function are not solely reliant on A β pathology. Likewise, our results on neuronal loss could only partly explain accelerated cognitive decline in PM-exposed *App*^{NL-G-F/+}-KI mice, though our findings are consistent with recent studies reporting a significant reduction of neuronal cell density by NeuN, Nissl, or H&E staining and reduced dendritic spines particularly in the entorhinal cortex, following PM exposure in various rodent models (Cacciottolo et al., 2017; Fonken et al., 2011; Lee et al., 2021; Patten et al., 2021). It is also worth discussing whether cognitive tests performed in the end of the exposure period had any impact on AD-like neuropathology in the brain.

Previous studies, for example, indicate that aberrant inflammation and the loss of BBB integrity are associated with PM exposure and neuropathologic consequences in animal models (Block and Calderon-Garciduenas, 2009; Calderon-Garciduenas et al., 2008; Campbell et al., 2009; Fonken et al., 2011; Haghani et al., 2020; Kleinman et al., 2008; Levesque et al., 2011). Both mechanisms are extensively being studied in AD. In fact, increased numbers of ambient particulates were found deposited in the brain of animals following chronic PM exposure (Patten et al., 2021). The increased permeability across BBB and/or inflammation elicited by those particulates in the brain are highly feasible toxic mechanisms of PM and other constituents of air pollution to promote neurodegeneration. Impaired BBB and microglia functions are also reported to exacerbate A β buildup in the brain (Deane et al., 2008; Keren-Shaul et al., 2017; Shibata et al., 2000; Ulrich et al., 2014), which may explain the increased A β plaques observed in older *App*^{NL-G-F/+}-KI mice exposed to PM.

Our current results demonstrate an accelerated transformation of glial cells from neuroprotective or homeostatic to harmful phenotypes. Microglia in various neurodegenerative diseases including AD are recently classified based on their unique transcriptomic signatures as TGF β -dependent homeostatic microglia and TREM2-dependent degenerative or disease-associated microglia (DAM) (Bonham et al., 2019; Butovsky et al., 2014). Disease-associated microglia are found to promote pathologic buildup and propagation of A β and tau, to increase the frequency of synapse loss, and to promote cognitive decline. More recently using single-cell RNA sequencing, microglia in the diseased brain are further divided up to 9 subsets with distinct transcriptomic signatures and coexist throughout the disease course (Morabito et al., 2021; Olah et al., 2020). The exact role of each subset of microglia in the disease progression, however, remains to be elucidated. Similarly, distinct astrocyte activation was also unveiled by transcriptomics. Proinflammatory DAM appears to promote transformation of homeostatic astrocytes (A0) to neurotoxic phenotypes (A1), which express high levels of complement C3 within astrocytes (Guttenplan et al., 2020; Liddelow et al., 2017). Interestingly, a recent study unveiled one mechanism by which neurotoxic astrocytes kill neurons through long-chain saturated lipids in APOE lipoparticles (Guttenplan et al., 2021). In our study, we sought to examine the change in the activation state of microglia and astrocytes following 12-week PM exposure and to assess whether any association with neuronal loss could be found.

Preliminary evidence using human AD brains shows that high expressions of ferritin, TREM2, or PU.1 in microglia are associated with DAM phenotypes (Kenkhuus et al., 2021; Rustenhoven et al., 2018) while high expression of Tmem119 and several other proteins are found in TGF β -dependent homeostatic microglia (Sato et al., 2016). Although our methods detecting potentially different activation phenotypes of glial cells are limited to immunostaining, we observed decreased prevalence of Tmem119+ microglia, increased prevalence of ferritin+ microglia and C3+ astrocytes particularly in cortex of PM-exposed animals at older age. We believe aging also play a significant role in the vulnerability of microglia and astrocytes to exogenous stimulants (ie, PM) as normal aging is sufficient to drive astrocytes towards neurotoxic phenotypes (Clarke et al., 2018). These findings strongly indicate that PM can promote microglia and astrocytes towards more harmful phenotypes leading to neurodegeneration. Additional studies (ie, transcriptomics approaches) will be required to validate our findings. In addition, the extent of such harmful glial population is also different in aged animals with or without plaques. Thus, how aging and AD pathology contribute to PM-induced neurotoxicity is key to better understand the risk of PM exposure on AD onset.

Our study has several limitations when it comes to translational significance and relevance to exposure and risk for humans. The VACES exposure system has several advantages, such as (1) providing a well-controlled exposure of concentrated ambient PM collected real-time during animal exposure periods and (2) providing exposure atmospheres containing toxic PM constituents at ratios consistent with their concentrations in ambient air, other exposure parameters (ie, duration of exposure [12 weeks] and the process and application of concentrated PM) deviate from real-life exposures to ambient air pollution in humans. Four-day exposure per week reflects typical air pollution episodes (Kleinman et al., 2005, 2007), and PM concentration given to animals was within the range of environmentally relevant concentrations for highly polluted areas (56–145 $\mu\text{g}/\text{m}^3$) (Calderon-Garciduenas et al., 2008; Kleinman et al., 2005, 2007; Moreno et al., 2008). In addition, exposing mice to higher particle concentrations than average human exposure is still translatable considering human heterogeneity of sensitivity to exposure, animal-to-human extrapolation, and the differences in exposure durations in humans (lifetime) and animal models (less than a lifetime) (Rees and Hattis, 1994). Intriguingly, a recent animal study used a mobile trailer equipped with temporary rodent vivarium in a heavily polluted site, to achieve environmentally relevant, unprocessed, and unconcentrated ambient air pollution exposure to the rat model (Patten et al., 2021). Unlike the VACES and other similar systems providing well-controlled exposure in the laboratory environment, this approach achieves a mean 24-h PM_{2.5} exposure at 15.6 $\mu\text{g}/\text{m}^3$, which is close to the US EPA's annual air quality standard of 12 $\mu\text{g}/\text{m}^3$. Although it is a given that exposure conditions that match closely to average exposures of humans are desired from the translational standpoint, despite the shorter exposure periods, behavioral differences between rodents and humans, and other limitations, it is still possible to draw valid translations between animal and human outcomes by carefully accounting for physiologic and biochemical differences and using appropriate dosimetry considerations when designing exposure procedures.

Secondly, particle concentrations during the 2 exposure periods (young and aged animals) differed due to the exposures being performed in different seasons of different years. The variability seen in the PM between these 2 cohorts may be attributed to high

atmospheric relative humidity levels (particle mass concentration of PM by VACES averaging $65.4 \mu\text{g}/\text{m}^3$ during the February–April months) which can decrease the efficiency of the particle concentrator due to unwanted hygroscopic growth of smaller PM in ambient environment. The average particle number concentration during the PM exposure in the aged animals was 2 times the value as in the young animals, but the average mass concentrations were constant between the 2 exposures suggesting ambient PM during the young age exposure was composed of a larger portion of smaller diameter particles than during the aged cohort exposure. As PM is typically considered more toxic and better able to infiltrate the body the smaller the size (Kim, 2001; Valavanidis et al., 2008), it remains to be examined to what degree this influenced the changes observed in AD phenotypes in *App^{NL-G-F/+}-KI* mice.

Lastly, our exposure scheme and behavior tests did not exclude a possibility that the completion of OLM and ORM positively or negatively affected neuropathology observed in each animal. However, it is important to note that a single training session does not affect AD-like pathology but that repeated behavioral training is necessary to reduce pathology including memory impairments, plaque burden, insoluble and soluble amyloid beta, as well as tauopathy (Billings et al., 2007). Other studies support these results and show that repeated physical or cognitive stimulation, over several months, alleviate memory decline, A β pathology, microgliosis, and rescue the levels of immediate early genes (Lazarov et al., 2005; Martinez-Coria et al., 2015; Mehla et al., 2022). In our study, since all animals were trained in the same way and for a shorter period of time compared with the reports just described, it was not likely that the behavioral tasks at the end of the exposure period had any significant impacts on neuropathology and, if any, training would have reduced pathology similarly in all *App^{NL-G-F/+}-KI* mice and would not have altered our observations.

In summary, our study echoes previous findings identified in various animal models showing accelerated AD phenotypes following PM exposure. Additional findings in the activation states of microglia and astrocytes may provide key insights into understanding the neurotoxic mechanisms of PM leading to cognitive decline and AD. This study suggests age, exposure duration, and exposure season could be important variables to take into consideration when conducting experiments using ambient PM. It is critical to recognize that air pollution is one of the prominent modifiable environmental risk factors in AD onset based on the recent growing evidence which highlights linkages between air pollution and AD. Public and environmental regulatory agencies may need to work to reduce air pollution to prevent further increase of dementia cases.

Supplementary data

Supplementary data are available at *Toxicological Sciences* online.

Declaration of conflicting interests

The authors declared no potential conflicts of interest with respect to the research, authorship, and/or publication of this article.

Funding

This study was supported by NIH R21 ES028496 (M.K.), RF1 NS130616 (M.K.), and the University of California, Irvine Institute

for Memory Impairments and Neurological Disorders (UCI MIND) Women's Alzheimer's Movement (WAM) Initiative Grant (M.K.).

References

- Bhatt, D. P., Puig, K. L., Gorr, M. W., Wold, L. E., and Combs, C. K. (2015). A pilot study to assess effects of long-term inhalation of airborne particulate matter on early Alzheimer-like changes in the mouse brain. *PLoS One* **10**, e0127102.
- Billings, L. M., Green, K. N., McGaugh, J. L., and LaFerla, F. M. (2007). Learning decreases A beta56 and tau pathology and ameliorates behavioral decline in 3xTg-AD mice. *J. Neurosci.* **27**, 751–761.
- Block, M. L., and Calderon-Garciduenas, L. (2009). Air pollution: Mechanisms of neuroinflammation and CNS disease. *Trends Neurosci.* **32**, 506–516.
- Bonham, L. W., Sirkis, D. W., and Yokoyama, J. S. (2019). The transcriptional landscape of microglial genes in aging and neurodegenerative disease. *Front. Immunol.* **10**, 1170.
- Bowe, B., Xie, Y., Yan, Y., and Al-Aly, Z. (2019). Burden of cause-specific mortality associated with PM2.5 air pollution in the United States. *JAMA Netw. Open* **2**, e1915834.
- Butovsky, O., Jedrychowski, M. P., Moore, C. S., Cialic, R., Lanser, A. J., Gabriely, G., Koeglsperger, T., Dake, B., Wu, P. M., Doykan, C. E., et al. (2014). Identification of a unique TGF-beta-dependent molecular and functional signature in microglia. *Nat. Neurosci.* **17**, 131–143.
- Cacciottolo, M., Wang, X., Driscoll, I., Woodward, N., Saffari, A., Reyes, J., Serre, M. L., Vizuete, W., Sioutas, C., Morgan, T. E., et al. (2017). Particulate air pollutants, APOE alleles and their contributions to cognitive impairment in older women and to amyloidogenesis in experimental models. *Transl. Psychiatry* **7**, e1022.
- Calderon-Garciduenas, L., Reed, W., Maronpot, R. R., Henriquez-Roldan, C., Delgado-Chavez, R., Calderon-Garciduenas, A., Dragustinovis, I., Franco-Lira, M., Aragon-Flores, M., Solt, A. C., et al. (2004). Brain inflammation and Alzheimer's-like pathology in individuals exposed to severe air pollution. *Toxicol. Pathol.* **32**, 650–658.
- Calderon-Garciduenas, L., Solt, A. C., Henriquez-Roldan, C., Torres-Jardon, R., Nuse, B., Herritt, L., Villarreal-Calderon, R., Osnaya, N., Stone, I., Garcia, R., et al. (2008). Long-term air pollution exposure is associated with neuroinflammation, an altered innate immune response, disruption of the blood-brain barrier, ultrafine particulate deposition, and accumulation of amyloid beta-42 and alpha-synuclein in children and young adults. *Toxicol. Pathol.* **36**, 289–310.
- Campbell, A., Araujo, J. A., Li, H., Sioutas, C., and Kleinman, M. (2009). Particulate matter induced enhancement of inflammatory markers in the brains of apolipoprotein E knockout mice. *J. Nanosci. Nanotechnol.* **9**, 5099–5104.
- Campbell, A., Oldham, M., Becaria, A., Bondy, S. C., Meacher, D., Sioutas, C., Misra, C., Mendez, L. B., and Kleinman, M. (2005). Particulate matter in polluted air may increase biomarkers of inflammation in mouse brain. *Neurotoxicology* **26**, 133–140.
- Carey, I. M., Anderson, H. R., Atkinson, R. W., Beevers, S. D., Cook, D. G., Strachan, D. P., Dajnak, D., Gulliver, J., and Kelly, F. J. (2018). Are noise and air pollution related to the incidence of dementia? A cohort study in London, England. *BMJ Open* **8**, e022404.
- Chang, K. H., Chang, M. Y., Muo, C. H., Wu, T. N., Chen, C. Y., and Kao, C. H. (2014). Increased risk of dementia in patients exposed to nitrogen dioxide and carbon monoxide: A population-based retrospective cohort study. *PLoS One* **9**, e103078.

- Chen, J. C., and Schwartz, J. (2009). Neurobehavioral effects of ambient air pollution on cognitive performance in US adults. *Neurotoxicology* **30**, 231–239.
- Clarke, L. E., Liddelow, S. A., Chakraborty, C., Munch, A. E., Heiman, M., and Barres, B. A. (2018). Normal aging induces A1-like astrocyte reactivity. *Proc. Natl. Acad. Sci. U.S.A.* **115**, E1896–E1905.
- Deane, R., Sagare, A., and Zlokovic, B. V. (2008). The role of the cell surface LRP and soluble LRP in blood-brain barrier Abeta clearance in Alzheimer's disease. *Curr. Pharm. Des.* **14**, 1601–1605.
- Fonken, L. K., Xu, X., Weil, Z. M., Chen, G., Sun, Q., Rajagopalan, S., and Nelson, R. J. (2011). Air pollution impairs cognition, provokes depressive-like behaviors and alters hippocampal cytokine expression and morphology. *Mol. Psychiatry* **16**, 987–995, 973.
- Gatto, N. M., Henderson, V. W., Hodis, H. N., St John, J. A., Lurmann, F., Chen, J. C., and Mack, W. J. (2014). Components of air pollution and cognitive function in middle-aged and older adults in Los Angeles. *Neurotoxicology* **40**, 1–7.
- Gonzalez-Maciel, A., Reynoso-Robles, R., Torres-Jardon, R., Mukherjee, P. S., and Calderon-Garciduenas, L. (2017). Combustion-derived nanoparticles in key brain target cells and organelles in young urbanites: Culprit hidden in plain sight in Alzheimer's disease development. *J. Alzheimers Dis.* **59**, 189–208.
- Guerra, R., Vera-Aguilar, E., Uribe-Ramirez, M., Gookin, G., Camacho, J., Osomio-Vargas, A. R., Mugica-Alvarez, V., Angulo-Olais, R., Campbell, A., Froines, J., et al. (2013). Exposure to inhaled particulate matter activates early markers of oxidative stress, inflammation and unfolded protein response in rat striatum. *Toxicol. Lett.* **222**, 146–154.
- Guttenplan, K. A., Stafford, B. K., El-Danaf, R. N., Adler, D. I., Munch, A. E., Weigel, M. K., Huberman, A. D., and Liddelow, S. A. (2020). Neurotoxic reactive astrocytes drive neuronal death after retinal injury. *Cell Rep.* **31**, 107776.
- Guttenplan, K. A., Weigel, M. K., Prakash, P., Wijewardhane, P. R., Hasel, P., Rufen-Blanchette, U., Munch, A. E., Blum, J. A., Fine, J., Neal, M. C., et al. (2021). Neurotoxic reactive astrocytes induce cell death via saturated lipids. *Nature* **599**, 102–107.
- Haghani, A., Cacciottolo, M., Doty, K. R., D'Agostino, C., Thorwald, M., Safi, N., Levine, M. E., Sioutas, C., Town, T. C., Forman, H. J., et al. (2020). Mouse brain transcriptome responses to inhaled nanoparticulate matter differed by sex and APOE in Nrf2-Nfkb interactions. *Elife* **9**, e54822.
- Harris, M. H., Gold, D. R., Rifas-Shiman, S. L., Melly, S. J., Zanobetti, A., Coull, B. A., Schwartz, J. D., Gryparis, A., Kloog, I., Koutrakis, P., et al. (2015). Prenatal and childhood traffic-related pollution exposure and childhood cognition in the project viva cohort (Massachusetts, USA). *Environ. Health Perspect.* **123**, 1072–1078.
- Herman, D. A., Wingen, L. M., Johnson, R. M., Keebaugh, A. J., Rensch, S. R., Hasen, I., Ting, A., and Kleinman, M. T. (2020). Seasonal effects of ambient PM2.5 on the cardiovascular system of hyperlipidemic mice. *J. Air Waste Manag. Assoc.* **70**, 307–323.
- Jedrychowski, W. A., Perera, F. P., Camann, D., Spengler, J., Butscher, M., Mroz, E., Majewska, R., Flak, E., Jacek, R., and Sowa, A. (2015). Prenatal exposure to polycyclic aromatic hydrocarbons and cognitive dysfunction in children. *Environ. Sci. Pollut. Res. Int.* **22**, 3631–3639.
- Jew, K., Herr, D., Wong, C., Kennell, A., Morris-Schaffer, K., Oberdorster, G., O'Banion, M. K., Cory-Slechta, D. A., and Elder, A. (2019). Selective memory and behavioral alterations after ambient ultrafine particulate matter exposure in aged 3xTgAD Alzheimer's disease mice. *Part. Fibre Toxicol.* **16**, 45.
- Karagulian, F., Belis, C. A., Dora, C. F. C., Pruss-Ustun, A. M., Bonjour, S., Adair-Rohani, H., and Amann, M. (2015). Contributions to cities' ambient particulate matter (PM): A systematic review of local source contributions at global level. *Atmos. Environ.* **120**, 475–483.
- Kenkhuis, B., Somarakis, A., de Haan, L., Dzyubachyk, O., IJsselsteijn, M. E., de Miranda, N. F. C. C., Lelieveldt, B. P. F., Dijkstra, J., van Roon-Mom, W. M. C., Höllt, T., et al. (2021). Iron loading is a prominent feature of activated microglia in Alzheimer's disease patients. *Acta Neuropathol. Commun.* **9**, 27.
- Keren-Shaul, H., Spinrad, A., Weiner, A., Matcovitch-Natan, O., Dvir-Szternfeld, R., Ulland, T. K., David, E., Baruch, K., Lara-Astaiso, D., Toth, B., et al. (2017). A unique microglia type associated with restricting development of Alzheimer's disease. *Cell* **169**, 1276–1290.e17.
- Kilian, J., and Kitazawa, M. (2018). The emerging risk of exposure to air pollution on cognitive decline and Alzheimer's disease - Evidence from epidemiological and animal studies. *Biomed. J.* **41**, 141–162.
- Kim, S., Jaques, P. A., Chang, M. C., Froines, J. R., and Sioutas, C. (2001). Versatile aerosol concentration enrichment system (VACES) for simultaneous in vivo and in vitro evaluation of toxic effects of ultrafine, fine and coarse ambient particles - Part I: Development and laboratory characterization. *J. Aerosol. Sci.* **32**, 1281–1297.
- Kim, S. H., Knight, E. M., Saunders, E. L., Cuevas, A. K., Popovech, M., Chen, L. C., and Gandy, S. (2012). Rapid doubling of Alzheimer's amyloid-beta40 and 42 levels in brains of mice exposed to a nickel nanoparticle model of air pollution. *F1000Res.* **1**, 70.
- Kleinman, M. T., Araujo, J. A., Nel, A., Sioutas, C., Campbell, A., Cong, P. Q., Li, H., and Bondy, S. C. (2008). Inhaled ultrafine particulate matter affects CNS inflammatory processes and may act via MAP kinase signaling pathways. *Toxicol. Lett.* **178**, 127–130.
- Kleinman, M. T., Hamade, A., Meacher, D., Oldham, M., Sioutas, C., Chakrabarti, B., Stram, D., Froines, J. R., and Cho, A. K. (2005). Inhalation of concentrated ambient particulate matter near a heavily trafficked road stimulates antigen-induced airway responses in mice. *J. Air Waste Manag. Assoc.* **55**, 1277–1288.
- Kleinman, M. T., Sioutas, C., Froines, J. R., Fanning, E., Hamade, A., Mendez, L., Meacher, D., and Oldham, M. (2007). Inhalation of concentrated ambient particulate matter near a heavily trafficked road stimulates antigen-induced airway responses in mice. *Inhal. Toxicol.* **19**(Suppl 1), 117–126.
- Latif-Hernandez, A., Shah, D., Craessaerts, K., Saido, T., Saito, T., De Strooper, B., Van der Linden, A., and D'Hooge, R. (2019). Subtle behavioral changes and increased prefrontal-hippocampal network synchronicity in APP(NL-G-F) mice before prominent plaque deposition. *Behav. Brain Res.* **364**, 431–441.
- Lazarov, O., Robinson, J., Tang, Y. P., Hairston, I. S., Korade-Mirnic, Z., Lee, V. M., Hersh, L. B., Sapolsky, R. M., Mirnic, K., and Sisodia, S. S. (2005). Environmental enrichment reduces Abeta levels and amyloid deposition in transgenic mice. *Cell* **120**, 701–713.
- Lee, S. H., Chen, Y. H., Chien, C. C., Yan, Y. H., Chen, H. C., Chuang, H. C., Hsieh, H. I., Cho, K. H., Kuo, L. W., Chou, C. C., et al. (2021). Three month inhalation exposure to low-level PM2.5 induced brain toxicity in an Alzheimer's disease mouse model. *PLoS One.* **16**, e0254587.
- Levesque, S., Taetzsch, T., Lull, M. E., Kodavanti, U., Stadler, K., Wagner, A., Johnson, J. A., Duke, L., Kodavanti, P., Surace, M. J., et al. (2011). Diesel exhaust activates and primes microglia: Air pollution, neuroinflammation, and regulation of dopaminergic neurotoxicity. *Environ. Health Perspect.* **119**, 1149–1155.
- Liddelow, S. A., Guttenplan, K. A., Clarke, L. E., Bennett, F. C., Bohlen, C. J., Schirmer, L., Bennett, M. L., Munch, A. E., Chung, W. S.,

- Peterson, T. C., et al. (2017). Neurotoxic reactive astrocytes are induced by activated microglia. *Nature* **541**, 481–487.
- Lin, H., Guo, Y., Zheng, Y., Zhao, X., Cao, Z., Rigdon, S. E., Xian, H., Li, X., Liu, T., Xiao, J., et al. (2017). Exposure to ambient PM_{2.5} associated with overall and domain-specific disability among adults in six low- and middle-income countries. *Environ. Int.* **104**, 69–75.
- Livingston, G., Huntley, J., Sommerlad, A., Ames, D., Ballard, C., Banerjee, S., Brayne, C., Burns, A., Cohen-Mansfield, J., Cooper, C., et al. (2020). Dementia prevention, intervention, and care: 2020 report of the Lancet Commission. *Lancet* **396**, 413–446.
- Luderer, U., Lim, J., Ortiz, L., Nguyen, J. D., Shin, J. H., Allen, B. D., Liao, L. S., Malott, K., Perraud, V., Wingen, L. M., et al. (2022). Exposure to environmentally relevant concentrations of ambient fine particulate matter (PM_{2.5}) depletes the ovarian follicle reserve and causes sex-dependent cardiovascular changes in apolipoprotein E null mice. *Part Fibre Toxicol.* **19**, 5.
- Martinez-Coria, H., Yeung, S. T., Ager, R. R., Rodriguez-Ortiz, C. J., Baglietto-Vargas, D., and LaFerla, F. M. (2015). Repeated cognitive stimulation alleviates memory impairments in an Alzheimer's disease mouse model. *Brain Res. Bull.* **117**, 10–15.
- Masuda, A., Kobayashi, Y., Kogo, N., Saito, T., Saido, T. C., and Itohara, S. (2016). Cognitive deficits in single App knock-in mouse models. *Neurobiol. Learn. Mem.* **135**, 73–82.
- Mathys, H., Davila-Velderrain, J., Peng, Z., Gao, F., Mohammadi, S., Young, J. Z., Menon, M., He, L., Abdurrob, F., Jiang, X., et al. (2019). Single-cell transcriptomic analysis of Alzheimer's disease. *Nature* **570**, 332–337.
- Mazzei, F., D'Alessandro, A., Lucarelli, F., Nava, S., Prati, P., Valli, G., and Vecchi, R. (2008). Characterization of particulate matter sources in an urban environment. *Sci. Total Environ.* **401**, 81–89.
- Mehla, J., Deibel, S. H., Karem, H., Hossain, S., Lacoursiere, S. G., Sutherland, R. J., Mohajerani, M. H., and McDonald, R. J. (2022). Dramatic impacts on brain pathology, anxiety, and cognitive function in the knock-in APP(NL-G-F) mouse model of Alzheimer disease following long-term voluntary exercise. *Alzheimers Res. Ther.* **14**, 143.
- Mehla, J., Lacoursiere, S. G., Lapointe, V., McNaughton, B. L., Sutherland, R. J., McDonald, R. J., and Mohajerani, M. H. (2019). Age-dependent behavioral and biochemical characterization of single APP knock-in mouse (APP(NL-G-F/NL-G-F)) model of Alzheimer's disease. *Neurobiol. Aging* **75**, 25–37.
- Meng, F. X., Hou, J. M., and Sun, T. S. (2017). In vivo evaluation of microglia activation by intracranial iron overload in central pain after spinal cord injury. *J. Orthop. Surg. Res.* **12**, 75.
- Misra, C., Kim, S., SHen, S., and Sioutas, C. (2002). A high flow rate, very low pressure drop impactor for inertial separation of ultrafine from accumulation mode particles. *J. Aerosol. Sci.* **33**, 735–752.
- Morabito, S., Miyoshi, E., Michael, N., Shahin, S., Martini, A. C., Head, E., Silva, J., Leavy, K., Perez-Rosendahl, M., and Swarup, V. (2021). Single-nucleus chromatin accessibility and transcriptomic characterization of Alzheimer's disease. *Nat. Genet.* **53**, 1143–1155.
- Moreno, T., Querol, X., Pey, J., Minguillon, M. C., Perez, N., Alastuey, A., Bernabe, R. M., Blanco, S., Cardenas, B., Eichinger, W., et al. (2008). Spatial and temporal variations in inhalable CuZnPb aerosols within the Mexico City pollution plume. *J. Environ. Monit.* **10**, 370–378.
- Morgan, T. E., Davis, D. A., Iwata, N., Tanner, J. A., Snyder, D., Ning, Z., Kam, W., Hsu, Y. T., Winkler, J. W., Chen, J. C., et al. (2011). Glutamatergic neurons in rodent models respond to nanoscale particulate urban air pollutants in vivo and in vitro. *Environ. Health Perspect.* **119**, 1003–1009.
- Oberdorster, G., Sharp, Z., Atudorei, V., Elder, A., Gelein, R., Kreyling, W., and Cox, C. (2004). Translocation of inhaled ultrafine particles to the brain. *Inhal. Toxicol.* **16**, 437–445.
- Olah, M., Menon, V., Habib, N., Taga, M. F., Ma, Y., Yung, C. J., Cimpean, M., Khairallah, A., Coronas-Samano, G., Sankowski, R., et al. (2020). Single cell RNA sequencing of human microglia uncovers a subset associated with Alzheimer's disease. *Nat. Commun.* **11**, 6129.
- Oudin, A., Forsberg, B., Adolfsson, A. N., Lind, N., Modig, L., Nordin, M., Nordin, S., Adolfsson, R., and Nilsson, L.-G. (2016). Traffic-related air pollution and dementia incidence in Northern Sweden: A longitudinal study. *Environ. Health Perspect.* **124**, 306–312.
- Patten, K. T., Valenzuela, A. E., Wallis, C., Berg, E. L., Silverman, J. L., Bein, K. J., Wexler, A. S., and Lein, P. J. (2021). The effects of chronic exposure to ambient traffic-related air pollution on Alzheimer's disease phenotypes in wildtype and genetically predisposed male and female rats. *Environ. Health Perspect.* **129**, 57005.
- Peeples, L. (2020). News feature: How air pollution threatens brain health. *Proc. Natl. Acad. Sci. U.S.A.* **117**, 13856–13860.
- Power, M. C., Weisskopf, M. G., Alexeeff, S. E., Coull, B. A., Spiro, A., 3rd., and Schwartz, J. (2011). Traffic-related air pollution and cognitive function in a cohort of older men. *Environ. Health Perspect.* **119**, 682–687.
- Ranft, U., Schikowski, T., Sugiri, D., Krutmann, J., and Kramer, U. (2009). Long-term exposure to traffic-related particulate matter impairs cognitive function in the elderly. *Environ. Res.* **109**, 1004–1011.
- Rees, C. D., and Hattis, D. (1994). Developing quantitative strategies for animal to human extrapolation. In *Principles and Methods of Toxicology*, 3rd ed. (A. W. Hayes, Ed), pp. 275–315. CRC Press.
- Reinert, A., Morawski, M., Seeger, J., Arendt, T., and Reinert, T. (2019). Iron concentrations in neurons and glial cells with estimates on ferritin concentrations. *BMC Neurosci.* **20**, 25.
- Rustenhoven, J., Smith, A. M., Smyth, L. C., Jansson, D., Scotter, E. L., Swanson, M. E. V., Aalderink, M., Coppieters, N., Narayan, P., Handley, R., et al. (2018). PU.1 regulates Alzheimer's disease-associated genes in primary human microglia. *Mol. Neurodegener.* **13**, 44.
- Saito, T., Matsuba, Y., Mihira, N., Takano, J., Nilsson, P., Itohara, S., Iwata, N., and Saido, T. C. (2014). Single App knock-in mouse models of Alzheimer's disease. *Nat. Neurosci.* **17**, 661–663.
- Satoh, J., Kino, Y., Asahina, N., Takitani, M., Miyoshi, J., Ishida, T., and Saito, Y. (2016). TMEM119 marks a subset of microglia in the human brain. *Neuropathology* **36**, 39–49.
- Shi, L., Wu, X., Danesh Yazdi, M., Braun, D., Abu Awad, Y., Wei, Y., Liu, P., Di, Q., Wang, Y., Schwartz, J., et al. (2020). Long-term effects of PM_{2.5} on neurological disorders in the American Medicare population: A longitudinal cohort study. *Lancet. Planet. Health.* **4**, e557–e565.
- Shibata, M., Yamada, S., Kumar, S. R., Calero, M., Bading, J., Frangione, B., Holtzman, D. M., Miller, C. A., Strickland, D. K., Ghiso, J., et al. (2000). Clearance of Alzheimer's amyloid-ss(1-40) peptide from brain by LDL receptor-related protein-1 at the blood-brain barrier. *J. Clin. Invest.* **106**, 1489–1499.
- Spangenberg, E., Severson, P. L., Hohsfield, L. A., Crapser, J., Zhang, J., Burton, E. A., Zhang, Y., Spevak, W., Lin, J., Phan, N. Y., et al. (2019). Sustained microglial depletion with CSF1R inhibitor impairs parenchymal plaque development in an Alzheimer's disease model. *Nat. Commun.* **10**, 3758.
- Tessum, C. W., Paoletta, D. A., Chambliss, S. E., Apte, J. S., Hill, J. D., and Marshall, J. D. (2021). PM_{2.5} pollutants disproportionately and

- systemically affect people of color in the United States. *Sci. Adv.* **7**, eabf4491. doi:10.1126/sciadv.abf4491.
- Ulrich, J. D., Finn, M. B., Wang, Y., Shen, A., Mahan, T. E., Jiang, H., Stewart, F. R., Piccio, L., Colonna, M., and Holtzman, D. M. (2014). Altered microglial response to Abeta plaques in APPPS1-21 mice heterozygous for TREM2. *Mol. Neurodegener.* **9**, 20.
- Valavanidis, A., Fiotakis, K., and Vlachogianni, T. (2008). Airborne particulate matter and human health: Toxicological assessment and importance of size and composition of particles for oxidative damage and carcinogenic mechanisms. *J. Environ. Sci. Health. C Environ. Carcinog. Ecotoxicol. Rev.* **26**, 339–362.
- Vogel-Ciernia, A., and Wood, M. A. (2014). Examining object location and object recognition memory in mice. *Curr. Protoc. Neurosci.* **69**, 8.31.1–8.31.17.
- Weuve, J., Puett, R. C., Schwartz, J., Yanosky, J. D., Laden, F., and Grodstein, F. (2012). Exposure to particulate air pollution and cognitive decline in older women. *Arch. Intern. Med.* **172**, 219–227.
- Woodward, N. C., Levine, M. C., Haghani, A., Shirmohammadi, F., Saffari, A., Sioutas, C., Morgan, T. E., and Finch, C. E. (2017). Toll-like receptor 4 in glial inflammatory responses to air pollution in vitro and in vivo. *J. Neuroinflammation* **14**, 84.
- Wu, T., Dejanovic, B., Gandham, V. D., Gogineni, A., Edmonds, R., Schauer, S., Srinivasan, K., Huntley, M. A., Wang, Y., Wang, T. M., et al. (2019). Complement C3 is activated in human AD brain and is required for neurodegeneration in mouse models of amyloidosis and tauopathy. *Cell Rep.* **28**, 2111–2123.e6.
- Zamanian, J. L., Xu, L., Foo, L. C., Nouri, N., Zhou, L., Giffard, R. G., and Barres, B. A. (2012). Genomic analysis of reactive astroglia. *J. Neurosci.* **32**, 6391–6410.
- Zhang, R., Wang, G., Guo, S., Zamora, M. L., Ying, Q., Lin, Y., Wang, W., Hu, M., and Wang, Y. (2015). Formation of urban fine particulate matter. *Chem. Rev.* **115**, 3803–3855.
- Zhang, X., Chen, X., and Zhang, X. (2018). The impact of exposure to air pollution on cognitive performance. *Proc. Natl. Acad. Sci. U.S.A.* **115**, 9193–9197.